

1 **Comparative transcriptomics analyses across species, organs and developmental stages reveal**
2 **functionally constrained lncRNAs**

3

4 Fabrice Darbellay^{1,§,*} and Anamaria Necsulea^{1,2,*}

5

6

7 ¹School of Life Sciences, École Polytechnique Fédérale de Lausanne (EPFL), Lausanne, Switzerland

8 ²Université de Lyon, Université Lyon 1, CNRS, Laboratoire de Biométrie et Biologie Évolutive UMR

9 5558, F-69622 Villeurbanne, France

10

11 [§]Present address: Environmental Genomics and Systems Biology Division, Lawrence Berkeley

12 National Laboratory, 1 Cyclotron Road, Berkeley, California 94720, USA.

13

14

15 *Corresponding authors:

16 Fabrice Darbellay (fabrice.darbellay@epfl.ch)

17 Anamaria Necsulea (anamaria.necsulea@univ-lyon1.fr)

18

19 Running title: Functionally constrained lncRNAs in embryonic development

20

21 Keywords: long non-coding RNAs; evolution; development; comparative transcriptomics.

22

23

24

25 **Abstract**

26 **Background** Transcription of long non-coding RNAs (lncRNAs) is pervasive, but their functionality is
27 disputed. As a class, lncRNAs show little selective constraint and negligible phenotypic effects upon
28 perturbation. However, key biological roles were demonstrated for individual lncRNAs. Most validated
29 lncRNAs were implicated in gene expression regulation, in pathways related to cellular pluripotency,
30 differentiation and organ morphogenesis, suggesting that functional lncRNAs may be more abundant
31 in embryonic development, rather than in adult organs.

32 **Results** Here, we perform a multi-dimensional comparative transcriptomics analysis, across five
33 developmental time-points (two embryonic stages, newborn, adult and aged individuals), four organs
34 (brain, kidney, liver and testes) and three species (mouse, rat and chicken). Overwhelmingly, lncRNAs
35 are preferentially expressed in adult and aged testes, consistent with the presence of permissive
36 transcription during spermatogenesis. lncRNAs are often differentially expressed among
37 developmental stages and are less abundant in embryos and newborns compared to adult individuals,
38 in agreement with a requirement for tighter expression control and less tolerance for noisy
39 transcription early in development. However, lncRNAs expressed during embryonic development
40 show increased levels of evolutionary conservation, both in terms of primary sequence and of
41 expression patterns, and in particular at their promoter regions. We find that species-specific lncRNA
42 transcription is frequent for enhancer-associated loci and occurs in parallel with expression pattern
43 changes for neighboring protein-coding genes.

44 **Conclusions** We show that functionally constrained lncRNA loci are enriched in developing organ
45 transcriptomes, and propose that many of these loci may function in an RNA-independent manner.

46

47 **Background**

48 Long non-coding RNAs (lncRNAs, loosely defined as transcripts that lack protein-coding potential, at
49 least 200 nucleotides long) are an excellent illustration of the ongoing conceptual tug-of-war between
50 biochemical activity and biological function (Graur et al. 2013; Doolittle 2018). The development of
51 sensitive transcriptome exploration techniques led to the identification of thousands of lncRNA loci in
52 vertebrates. While this ever wider class of transcripts includes well-studied lncRNAs with undisputed
53 biological roles, such as *Xist* (Brown et al. 1991) or *H19* (Brannan et al. 1990), experimental validations
54 are lacking for the great majority of lncRNAs and their functionality is controversial.

55

56 The first functional characterizations of individual lncRNAs forged the idea that these non-coding
57 transcripts are important contributors to gene expression regulatory networks. This has been
58 unequivocally proven for some lncRNAs, such as *Xist*, whose transcription and subsequent coating of
59 the X chromosome triggers a complex chain of molecular events leading to X inactivation in placental
60 mammals (Gendrel and Heard 2014). Additional proposed mechanisms for gene expression regulation
61 by lncRNAs included directing chromatin-modifying complexes at specific genomic locations, to control
62 gene expression in *trans* (Rinn et al. 2007); providing decoy targets for microRNAs (Cesana et al. 2011);
63 enhancing expression of neighboring genes through an RNA-dependent mechanism (Ørom et al. 2010).
64 These initial studies generally asserted that the biological function of lncRNA loci is directly carried out
65 by the transcribed RNA molecule. However, it rapidly became evident that in some cases the function
66 resides in the act of transcription at a given genomic location, rather than in the product of
67 transcription (Latos et al. 2012). In recent years, this view has gained ground, with several publications
68 showing that lncRNA transcripts are not required, and that instead biological functions are carried out
69 by other elements embedded in the lncRNA genomic loci (Bassett et al. 2014). For example, it was
70 recently shown that transcription of the *Linc-p21* gene, originally described as a *cis*-acting enhancer
71 lncRNA, is not needed to regulate neighboring gene expression (Groff et al. 2016). Genetic engineering
72 of multiple lncRNA loci in mouse likewise showed that lncRNA transcripts are dispensable, and that

73 gene expression regulation by lncRNA loci is instead achieved by the process of lncRNA transcription
74 and splicing, or by additional regulatory elements found in lncRNA promoters (Engreitz et al. 2016;
75 Anderson et al. 2016). Furthermore, some attempts to look for lncRNA function through genetic
76 engineering approaches showed that the tested lncRNA loci are altogether dispensable (Amândio et
77 al. 2016; Zakany et al. 2017; Goudarzi et al. 2019). These recent observations signal a paradigm shift in
78 lncRNA biology, as it is increasingly acknowledged that, even when phenotypic effects can be
79 unambiguously mapped to lncRNA loci, the underlying biological processes are not necessarily driven
80 by the lncRNA transcripts themselves.

81
82 Importantly, this new perspective on lncRNA biology had been predicted by evolutionary analyses,
83 which have long been used to evaluate the functionality of diverse genomic elements (Haerty and
84 Ponting 2014; Ulitsky 2016). Evolutionary studies of lncRNAs in vertebrates all agree that the extent of
85 selective constraint on lncRNA primary sequences is very low, though significantly above the genomic
86 background (Ponjavic et al. 2007; Kutter et al. 2012; Necsulea et al. 2014; Washietl et al. 2014; Hezroni
87 et al. 2015). These observations are compatible with the hypothesis that many of the lncRNAs detected
88 with sensitive transcriptomics techniques may be non-functional noise (Ponjavic et al. 2007), but may
89 also indicate that lncRNA functionality does not reside in the primary transcribed sequence. In
90 contrast, mammalian lncRNA promoters show higher levels of sequence conservation, similar to
91 protein-coding gene promoters, as expected if they carry out enhancer-like regulatory functions
92 independently of the transcribed RNA molecule. Moreover, it was previously reported that, in multi-
93 exonic lncRNAs, splicing signals are more conserved than the rest of the exonic sequence (Schüler et
94 al. 2014; Haerty and Ponting 2015), which is compatible with the recent finding that lncRNA splicing
95 can contribute to neighboring gene regulation (Engreitz et al. 2016). Thus, detailed evolutionary
96 analyses of lncRNA loci can bring important insights into their functionality, and can help to prioritize
97 candidates for experimental validation.

98

99 At present, comparative transcriptomics analyses in vertebrates agree that the extent of evolutionary
100 conservation of lncRNA sequences and expression patterns is very limited. However, these studies
101 were so far restricted to adult organ transcriptomes. In particular, it was shown that most known
102 vertebrate lncRNAs are active in adult testes and thus likely during spermatogenesis, a process
103 characterized by a permissive chromatin environment, which can promote non-functional
104 transcription (Soumillon et al. 2013). The resulting lncRNA datasets may thus be enriched in non-
105 functional transcripts. Additional lines of evidence suggest that the search for functional lncRNAs
106 should be extended beyond adult organ transcriptomes. For example, involvement in developmental
107 phenotypes was proposed for many experimentally-tested lncRNAs (Sauvageau et al. 2013; Ulitsky et
108 al. 2011; Grote et al. 2013), and an enrichment for developmental transcription factor binding was
109 reported for the promoters of highly conserved lncRNAs (Necsulea et al. 2014). These observations
110 motivated us to add a temporal dimension to comparative lncRNA transcriptomics studies. Therefore,
111 we characterize here the lncRNA transcriptomes of two model mammalian species (mouse and rat), in
112 four major organs (brain, kidney, liver and testes), across five developmental stages that cover the
113 entire lifespan of the individuals (including two embryonic stages, newborn, young adult and aged
114 individuals). To gain a deeper evolutionary perspective, we generate similar data for embryonic stages
115 of chicken somatic organs. We analyze the spatial and temporal expression patterns of protein-coding
116 and lncRNA genes, in conjunction with their evolutionary conservation. We find that, while lncRNAs
117 are overall poorly conserved among species in terms of primary sequence or expression patterns,
118 higher frequencies of evolutionarily constrained lncRNAs are observed in embryonic transcriptomes.
119 For many of these loci, biological function may be RNA-independent, as the highest levels of sequence
120 conservation are observed on promoter regions and on splice signals, rather than on lncRNA exonic
121 sequence. Our results are thus compatible with unconventional, RNA-independent functions for
122 lncRNA loci, in particular for those that are expressed during embryonic development.

123 **Results**

124 *Comparative transcriptomics across species, organs and developmental stages*

125 To study protein-coding and lncRNA expression patterns across both developmental and evolutionary
126 time, we generated RNA-seq data for mouse and rat, for four major organs (brain, kidney, liver and
127 testes) and five developmental time points, including two embryonic stages, newborn, young and aged
128 adult individuals (Figure 1A, Supplementary Table 1, Methods). The selected time points allow us to
129 obtain a broad view of major organ ontogenesis and to capture drastic physiological changes during
130 development (Theiler 1989). We chose to include in our study both young adult (8-10 weeks old) and
131 aged adult individuals (12 to 24 months old), to investigate transcriptomic changes that occur later in
132 life, thus completing our overview of the temporal patterns of gene expression variation. At the
133 earliest embryonic stage (day 13.5 post-conception for mouse, day 15 for rat), only three of the four
134 studied organs, with the exception of the testes, are well differentiated and large enough to be readily
135 dissected. Our experimental design for mouse and rat thus comprises 19 organ / developmental stage
136 combinations. Although most of our study relies on mouse-rat comparisons, to obtain a broader
137 evolutionary perspective we generated comparable RNA-seq data for the chicken, for the two earliest
138 developmental stages (Figure 1A, Supplementary Table 1). We obtained between 2 and 4 biological
139 replicates for each species/organ/developmental stage combination (Supplementary Table 1).
140 Additional RNA-seq samples from previous publications were included in the lncRNA annotation
141 pipeline, to increase detection sensitivity (Supplementary Table 2, Methods).

142
143 The organs and developmental stages included in our study differ greatly in terms of their cellular
144 composition diversity. To verify that our whole-organ RNA-seq data reflects cellular composition
145 heterogeneity, we assessed the expression patterns of cell population markers derived from single-
146 cell transcriptomics studies (Tabula Muris Consortium 2018; Green et al. 2018) in our samples (Figure
147 1B, Supplementary Table 3). This analysis confirms that our transcriptome collection reflects expected
148 developmental patterns. For example, mature oligodendrocyte cell markers are systematically highly

149 expressed in adult brain, while oligodendrocyte precursor markers are more highly expressed in the
150 earliest developmental stages (Figure 1B). Similarly, *Neurod6*, a gene involved in neuronal
151 differentiation (Kathleen Baxter et al. 2009), is preferentially expressed in embryonic and newborn
152 brain. Moreover, spermatogenesis-specific markers are enriched in adult but not in embryonic and
153 newborn testes, while markers for somatic cells (Leydig, Sertoli cells) are expressed earlier during
154 testes development (Figure 1B). Immune cell markers tend to be more broadly shared across organs
155 and developmental stages, but show strongest expression in the late embryo and newborn liver (Figure
156 1B), consistent with this organ's crucial role in establishing immunity (Nakagaki et al. 2018). In general,
157 adult organ transcriptomes contain higher numbers of expressed cell type-specific markers (Figure 1B).
158 However, as these genes were defined based on adult organ data, this observation may indicate that
159 cell sub-populations that are specific to embryonic organs are under-represented in this marker set,
160 rather than reflecting the true cellular diversity at different developmental stages.

161

162 We note that, in some cases, the cell type-specific markers predicted by single-cell transcriptomics
163 studies have seemingly unexpected expression patterns in our whole-organ RNA-seq collection. For
164 example, the expression of *Parvalbumin (Pvalb)*, which was proposed as a marker for collecting duct
165 epithelial cells in the kidney (Tabula Muris Consortium 2018), is highest in the adult and aged brain,
166 for both mouse and rat (Figure 1B). Likewise, cellular retinoic acid binding protein 1 (*Crabp1*), which
167 was predominantly detected in spermatogonia in a single-cell transcriptomics study of mouse testes
168 (Green et al. 2018), is preferentially expressed in mid-stage embryonic kidney in our samples (Figure
169 1B). These apparent discrepancies likely reflect the pleiotropic nature of genes, as well as the presence
170 of similar cell types across organs with distinct physiological functions (Arendt et al. 2016).

171

172 Finally, the genes proposed as markers for major cell types generally behave similarly in mouse and
173 rat, although some species-specific patterns can be observed, in particular for immune cell markers
174 (Figure 1B). Likewise, for those genes that had orthologues in the chicken, expression patterns are

175 generally similar among species, with higher between-species divergence for immunity-related genes
176 (Supplementary Figure 1). This observation confirms that the organs and developmental stages
177 selected for our integrative transcriptomics study are comparable across species.

178

179 Overall, these results indicate that our whole-organ transcriptomics collection provides a good
180 overview of the cell composition changes that occur during development, and enables meaningful
181 comparisons across species.

182 *Variations in transcriptome complexity among organs and developmental stages*

183 We next sought to assess transcriptome complexity in different organs across developmental stages,
184 for both protein-coding genes and lncRNAs. To predict lncRNAs, we used the RNA-seq data to
185 reconstruct gene models with StringTie (Pertea et al. 2015), building on existing genomic annotations
186 (Cunningham et al. 2019). We verified the protein-coding potential of newly annotated transcripts,
187 based on the codon substitution frequency score (Lin et al. 2007, 2011) and on sequence similarity
188 with known proteins, and we applied a stringent series of filters to reduce contaminations from un-
189 annotated protein-coding UTRs and other artefacts (Methods). We thus obtain a total of 18,858
190 candidate lncRNAs in the mouse, 20,159 in the rat and 5,496 in the chicken, including both newly-
191 annotated and previously known lncRNAs transcribed in our samples (Supplementary Dataset 1). We
192 note that many of these candidate lncRNAs are expressed at very low levels. When imposing a
193 minimum normalized expression level (transcript per million, or TPM) at least equal to 1, in at least
194 one sample, the numbers of candidate lncRNAs falls to 12,199, 15,319 and 2,892 in the mouse, rat and
195 chicken, respectively (Supplementary Datasets 2-3, Supplementary Table 4).

196

197 The differences in lncRNA content among species may reflect discrepancies in RNA-seq read coverage
198 and sample distribution, as well as genome sequence and annotation quality. To correct for the effect
199 of RNA-seq read coverage, we down-sampled the RNA-seq data to obtain the same number of uniquely
200 mapped reads for each organ/developmental stage combination within each species (Methods). After

201 this equalizing procedure, the number of detectable protein-coding genes (supported by at least 10
202 uniquely mapped reads) still shows broad variations among organs and developmental stages, with
203 the highest numbers of genes detected in the testes, for all time points (Figure 1C). Large numbers of
204 protein-coding genes (between 12,800 and 16,700) are detected in all samples. In contrast, for
205 lncRNAs, the pattern is much more striking: the young and aged adult testes express between 11,000
206 and 12,000 lncRNAs, in both mouse and rat, while in somatic organs and earlier developmental stages
207 we can detect only between 1,800 and 4,800 lncRNAs (Figure 1D). This observation is in agreement
208 with previous findings indicating that the particular chromatin environment of the adult testes, and in
209 particular of spermatogenesis-specific cell types, is extraordinarily permissive to transcription
210 (Soumillon et al. 2013). Interestingly, the numbers of protein-coding genes detectable in each organ
211 also varies among developmental stages. In young and aged adult individuals, the brain shows the
212 second-highest number of expressed protein-coding genes, after the testes, as previously observed
213 (Soumillon et al. 2013; Ramsköld et al. 2009). However, in embryonic and newborn samples, the kidney
214 expresses higher numbers of protein-coding genes than the brain (Figure 1C).

215 *Developmental expression patterns are well conserved among species for protein-coding genes*

216 Broad patterns of transcriptome evolution are already visible in our analyses of cell type specific
217 markers and of transcriptome complexity: individual gene expression profiles and numbers of
218 expressed genes are generally similar between mouse and rat, while more divergence is observed
219 between the two rodent species and the chicken (Figure 1B-D, Supplementary Figure 1). To further
220 explore the evolution of developmental gene expression patterns, we performed a principal
221 component analysis (PCA) on normalized, log-transformed TPM values for 10,363 protein-coding
222 genes shared among the three species (Methods, Figure 2A). This analysis revealed that the main
223 source of gene expression variability among species, organs and developmental stages is the
224 distinction between adult and aged testes and the other samples, which are separated on the first PCA
225 axis (Figure 2A). In contrast, embryonic and newborn testes are grouped with kidney samples from
226 similar developmental stages, in agreement with the common developmental origin of the kidney and

227 the gonads (McMahon 2016). The first axis of the PCA, which explains 67% of the total expression
228 variance, also correlates with the developmental stage: samples derived from adult and aged
229 individuals have higher coordinates on this axis than embryonic and newborn samples, for mouse and
230 rat (Figure 2A). The second PCA axis (10% explained variability) mainly reflects the difference between
231 brain and the other organs (Figure 2A). While mouse and rat samples are generally undistinguishable,
232 the PCA confirms that there is considerably higher expression divergence between chicken and the
233 two rodent species (Figure 2A). However, differences among major organs are stronger than
234 differences among species, even at these broad evolutionary distances: brain samples all cluster
235 together, irrespective of the species of origin, and are clearly separated from kidney and liver samples
236 on the second PCA axis (Figure 2A). Interestingly, within the brain cluster, embryonic chicken samples
237 tend to be closer to adult and aged rodent brains than to embryonic or neonate samples (Figure 2A).

238

239 These broad patterns of gene expression variations among species, organs and developmental stages
240 are confirmed by a hierarchical clustering analysis based on Spearman's correlation coefficients
241 between pairs of samples (Figure 2B). The strongest clustering is observed for adult and aged testes
242 samples, followed by a robust grouping of brain samples, irrespective of the species (Figure 2B).

243

244 For the mouse and rat, we could delve deeper into the evolutionary conservation of gene expression
245 patterns, by asking whether variations among developmental stages are shared between species. We
246 used models from the DESeq2 (Love et al. 2014) package to detect differential gene expression among
247 developmental stages, independently for each species and organ (Supplementary Dataset 4,
248 Methods). As expected given the wide range of developmental stages that we sampled, the great
249 majority of protein-coding genes are significantly differentially expressed ($FDR < 0.01$) among stages, in
250 each organ (Supplementary Dataset 4). We selected orthologous protein-coding genes that are
251 differentially expressed (DE) in both species, and used the K-means clustering algorithm to discover
252 broad patterns of variations among species and stages (Methods). In general, differentially expressed

253 genes show parallel patterns of variation among developmental stages in mouse and rat, for somatic
254 organs (Figure 2C, Supplementary Figure 2). Genes with shared patterns of variation among
255 developmental stages are enriched in organ-specific functional categories, such as nervous system
256 development and axon guidance for the first cluster of genes presented in Figure 2C, which have high
257 expression levels in the embryonic and newborn samples (Supplementary Dataset 4). While temporal
258 expression variations are generally conserved between species for brain, kidney and liver, almost 25%
259 of differentially expressed genes show different trends for mouse and rat in the testes (Supplementary
260 Figure 2). These sets of genes do not show any strong functional enrichment (Supplementary Dataset
261 4). This pattern confirms previous reports indicating that gene expression evolution is faster in the
262 adult testes (Brawand et al. 2011), and extends them by showing that patterns of variations among
263 developmental stages are often species-specific in the testes.

264 *Spatial and temporal expression pattern differences between protein-coding genes and lncRNAs*

265 We next compared spatial and temporal expression patterns between protein-coding genes and
266 lncRNAs. In agreement with previous findings -----, we show that lncRNAs are overwhelmingly
267 preferentially expressed in the testes (Figure 3A). Indeed, more than 68% of lncRNAs reach their
268 maximum expression level in this organ, compared to only approximately 32% of protein-coding genes,
269 for both mouse and rat (Figure 3A). Interestingly, more than 80% of lncRNAs are preferentially
270 expressed in young and aged adult samples, compared to only 62% of protein-coding genes (Figure
271 3B).

272

273 As noted previously, between 59 and 82% of protein-coding genes are significantly differentially
274 expressed (DE) among developmental stages, at a false discovery rate (FDR) below 1%, in each organ
275 and species (Figure 3C, Supplementary Dataset 4). The proportions of DE lncRNAs are much lower in
276 somatic organs, between 18 and 40%, but are similar in the testes, around 75% (Figure 3C). However,
277 we suspected that this could be due to the low expression levels of this class of genes, as total read
278 counts are known to affect the sensitivity of DE analyses (Anders and Huber 2010). Indeed, as

279 previously observed, lncRNAs are expressed at much lower levels and in fewer organ/developmental
280 stage combinations than protein-coding genes (Supplementary Figure 3A-C). To control for this effect,
281 we down-sampled the read counts observed for protein-coding genes, bringing them to the same
282 average counts as lncRNAs but preserving relative gene abundance (Methods). Strikingly, when
283 performing the DE analysis on this dataset, we observe higher proportions of DE loci for lncRNAs
284 compared to protein-coding genes (Figure 3C). Moreover, the amplitude of expression variation
285 among developmental stages are more important for lncRNAs than for protein-coding genes
286 (Supplementary Figure 3D). This is expected given the lower lncRNA expression levels, which preclude
287 detecting subtle expression shifts among time points. Finally, we observe that the developmental
288 stage with maximum expression is generally different between protein-coding genes and lncRNAs,
289 even when considering genes that are significantly DE among stages. For all organs, DE lncRNAs tend
290 to show highest expression levels in the young and aged adults, while DE protein-coding genes are
291 more homogeneously distributed among developmental stages (Figure 3D, Supplementary Figure 3E).

292

293 Similar conclusions are reached when performing DE analyses between consecutive time points
294 (Supplementary Dataset 4). For both protein-coding genes and lncRNAs, the strongest expression
295 changes are observed between newborn and young adult individuals. Almost 10,000 lncRNAs are
296 significantly up-regulated between newborn and young adult testes, confirming the strong enrichment
297 for lncRNAs during spermatogenesis (Supplementary Dataset 4). We note that, as expected, the lowest
298 numbers of DE genes are observed at the transition between young and aged adult organs. At this
299 time-point, we observe more changes for the rat than for the mouse, potentially due to a higher
300 proportion of immune cell infiltrates in rat aged organs. Genes associated with antigen processing and
301 presentation tend to be expressed at higher levels in aged adults than in young adults, for mouse
302 kidney, rat brain and liver (Supplementary Dataset 4).

303 *Stronger selective constraint on lncRNAs expressed earlier in development*

304 We next analyzed the patterns of long-term evolutionary sequence conservation for lncRNAs, in
305 conjunction with their spatio-temporal expression pattern (Supplementary Table 5). We used the
306 PhastCons score (Siepel et al. 2005) across placental mammals (Casper et al. 2018), to assess the level
307 of sequence conservation for various aspects of mouse lncRNAs: exonic sequences, promoter regions
308 (defined as 1 kb regions upstream of the transcription start site, masking any exonic sequence within
309 this region), splice sites (first and last two bases of the introns, for multi-exonic loci). As approximately
310 20% of lncRNAs overlap with exonic regions from other genes on the opposite strand (Supplementary
311 Dataset 1), we masked exonic sequences from other genes before computing sequence conservation
312 scores. We analyzed sets of protein-coding genes and lncRNAs that are expressed above noise levels
313 (TPM \geq 1, averaged across all replicates) in each organ / developmental stage combination.

314

315 For exonic sequences and splice site regions, the extent of sequence conservation is much lower for
316 lncRNAs than for protein-coding genes, irrespective of the organ and developmental stage in which
317 they are expressed (Figure 4A, C). In contrast, promoter sequence conservation levels are more
318 comparable between protein-coding genes and lncRNAs (Figure 4B). For all examined regions and for
319 both categories of genes, the spatio-temporal expression pattern is well correlated with the level of
320 sequence conservation. Globally, sequence conservation is higher for genes that are expressed earlier
321 in development than for genes expressed later in development, and is significantly higher for somatic
322 organs than for adult and aged testes (Figure 4). Interestingly, for genes that are highly expressed in
323 mid-stage embryonic brain and kidney samples, the levels of promoter sequence conservation are
324 higher for lncRNAs than for protein-coding genes (Figure 4B). We also observed that lncRNAs that are
325 transcribed from bidirectional promoters tend to have higher sequence conservation levels than other
326 lncRNAs (Supplementary Figure 4).

327

328 Finally, we asked whether the highest level of evolutionary sequence conservation is seen at exons,
329 promoter or splice site regions, for each lncRNA locus taken individually. We show that this pattern
330 also depends on the organs and the developmental stages where the lncRNAs are expressed: for loci
331 detected in somatic organs and in the developing testes, there is significantly higher conservation for
332 the promoter and the splice sites than for exonic regions (Supplementary Figure 4). However, for
333 lncRNAs that are highly transcribed in the adult and aged testes (which constitutes the great majority
334 of genes), this pattern is absent (Supplementary Figure 4).

335 Detection of homologous lncRNAs across species

336 Having investigated the patterns of long-term sequence conservation of mouse lncRNAs, we next
337 sought to assess the conservation of lncRNA repertoires in mouse, rat and chicken. We detected
338 lncRNA separately in each species, using only RNA-seq data and existing genome annotations, as
339 previously suggested (Hezroni et al. 2015). We then searched for putative 1-to-1 orthologous lncRNAs
340 between species using pre-computed whole-genome alignments as a guide (Methods), to increase the
341 sensitivity of orthologous gene detection in the presence of rapid sequence evolution (Washietl et al.
342 2014). The orthologous lncRNA detection procedure involves several steps, including the identification
343 of putative homologous (projected) loci across species, filtering to remove large-scale structural
344 changes in the loci and intersection with predicted loci in the target species (Methods). As illustrated
345 in Figure 5, for comparisons between rodents the extent of sequence divergence is low enough that
346 more than 90% of 12,199 high-confidence lncRNA loci (expressed at TPM \geq 1 in at least one sample)
347 are successfully projected from mouse to rat (Figure 5A, Supplementary Dataset 5). However, only 53%
348 of projected loci have even weak levels of detectable transcription in the target species (at least 10
349 uniquely mapped reads). Only 27% of mouse lncRNA loci have predicted 1-to-1 orthologues in the rat,
350 and only 18% are orthologous to confirmed lncRNA loci in the rat (Figure 5A, Supplementary Dataset
351 5). The 1,081 mouse lncRNAs that have non-lncRNAs orthologues in the rat are generally matched with
352 loci discarded because of low read coverage, minimum exonic length or distance to protein-coding

353 genes (Supplementary Dataset 5). Cases of lncRNA-protein-coding orthologues are rare at this
354 evolutionary distance (Supplementary Dataset 5), and they may stem from gene classification errors.

355
356 At larger evolutionary distances, the rate of sequence evolution is the main factor hampering detection
357 of orthologous lncRNAs. Only 1,940 (16%) of mouse high-confidence lncRNAs (TPM \geq 1) could be
358 projected onto the chicken genome, and after subsequent filters we detect only 56 mouse – chicken
359 lncRNA orthologues (Figure 5A, Supplementary Dataset 5). We note that our lncRNA detection power
360 is likely weaker for the chicken than for the rodents because of organ and developmental stage
361 sampling, although we did strive to include RNA-seq data from adult organs in the lncRNA detection
362 process (Methods, Supplementary Table 2).

363
364 Conserved lncRNAs differ from non-conserved lncRNAs in terms of expression patterns. While only
365 subtle differences can be observed when comparing mouse-rat orthologous lncRNAs to the mouse-
366 specific lncRNA set, lncRNAs that are conserved across mouse, rat and chicken are dramatically
367 enriched in somatic organs and early developmental stages (Figure 5B,C, Supplementary Table 6).
368 Although their expression patterns have a strong species-specific component, shared patterns of organ
369 specificity can be detected (Supplementary Figure 5).

370 *Global patterns of lncRNA expression across species, organs and developmental stages*

371 We next assessed the global patterns of expression variation across species, organs and developmental
372 stages, for predicted mouse – rat lncRNA orthologues (Supplementary Dataset 6). As for protein-coding
373 genes, the main source of variability in a PCA performed on lncRNA expression levels is the difference
374 between adult and aged testes and the other samples (Figure 6A, Supplementary Figure 6). However,
375 for lncRNAs samples cluster according to the species of origin already on the second factorial axis (10%
376 explained variance), thus confirming that lncRNA expression patterns evolve rapidly. Overall,
377 differences between organs and developmental stages are less striking for lncRNAs, compared to the
378 variation stemming from the species factor (Figure 6A, Supplementary Figure 6). This pattern is also

379 visible on a hierarchical clustering analysis (performed on distances derived from Spearman's
380 correlation coefficient): in contrast with what is observed for protein-coding genes, for lncRNAs
381 samples generally cluster by species, with the exception of adult and aged testes which are robustly
382 grouped.

383

384 The higher rates of lncRNA expression evolution are also visible when analyzing within-species
385 variations, through comparisons across biological replicates (Figure 7A). We sought to measure the
386 global extent of gene expression conservation, by contrasting between-species and within-species
387 variations. Briefly, we constructed an expression conservation index by dividing the between-species
388 and the within-species Spearman's correlation coefficient, computed on all genes from a category, for
389 a given organ / developmental stage combination (Methods). The resulting expression conservation
390 values are very high for protein-coding genes, in particular for the brain and the mid-stage embryonic
391 kidney. However, there is significant less conservation between species for the adult and aged testes
392 (Figure 7B). For lncRNAs, expression conservation values are much lower than those observed for
393 protein-coding genes, with strikingly low values for adult and aged testes (Figure 7C).

394 *Evolutionary divergence of individual lncRNA expression profiles*

395 Having established that, globally, lncRNA expression patterns evolve very rapidly, we next sought to
396 assess expression divergence at the individual gene level. We first asked whether temporal patterns
397 of expression variations are conserved across rodent species. We selected lncRNAs that are
398 significantly differentially expressed (FDR<0.01) across developmental stages, in both mouse and rat
399 (Supplementary Dataset 4), and grouped them into clusters (Methods). We observed that in general,
400 lncRNAs show consistent patterns of variation among developmental stage in mouse and rat, with a
401 few exceptions in the kidney and liver (Supplementary Figure 7). Interestingly, lncRNAs that are DE in
402 the testes only rarely show divergent profiles between species, in contrast with what is observed for
403 protein-coding genes, where 25% of genes have different temporal patterns for mouse and rat

404 (Supplementary Figures 2,7). Overwhelmingly, lncRNAs are more highly expressed in adult and aged
405 testes than in developing testes, in both mouse and rat.

406

407 To further quantify lncRNA expression profile differences among species, we measured the amount of
408 expression divergence as the Euclidean distance between relative expression profiles (average TPM
409 values across biological replicates, normalized by dividing by the sum of all values for a gene, for each
410 species), for mouse and rat orthologues (Methods, Supplementary Dataset 7, Supplementary Table 7).

411 The resulting expression divergence values correlate negatively with the average expression level
412 (Figure 8A), as expected. While the raw expression divergence values are significantly higher for

413 lncRNAs than for protein-coding genes (Figure 8B), this is largely due to the low lncRNA expression
414 levels. Indeed, the effect disappears when analyzing the residual expression divergence after

415 regressing the mean expression level (Figure 8C). For lncRNAs, we also observe a weak negative
416 correlation between expression divergence and the extent of exonic sequence conservation (Figure

417 8D). We measured the relative contribution of each organ/developmental stage to the expression
418 divergence estimate (Figure 8E). For both protein-coding genes and lncRNAs, by far the highest

419 contributors are the young adult and aged testes samples, which are responsible for almost 30% of the
420 lncRNA expression divergence (Figure 8E). This is visible in the expression patterns of the 2 protein-

421 coding and lncRNA genes with the highest residual expression divergence: the lncRNA expression
422 divergence is mostly due to changes in adult testes, while more complex expression pattern changes

423 seem to have occurred for the protein-coding genes (Supplementary Figure 8). The most divergent
424 protein-coding genes are enriched in functions related to immunity (Supplementary Dataset 7).

425 Candidate species-specific lncRNAs

426 We next sought to investigate the most extreme cases of expression divergence: situations where
427 expression can be robustly detected in one species, but not in the other one, despite the presence of

428 perfect sequence alignment (Methods). We selected lncRNA loci that were supported by at least 100
429 uniquely mapped reads in one species, with no reads detected in the predicted homologous region in

430 the other species. With this convention, we obtain 1,041 candidate mouse-specific and 1,646
431 candidate rat-specific loci (Supplementary Dataset 8). These lists include striking examples, such as the
432 region downstream of the *Fzd4* protein-coding gene, which contains a mouse-specific and a rat-specific
433 lncRNA candidate, each perfectly aligned in the other species (Supplementary Figure 9A). We could
434 not identify any differential transcription factor binding or transposable element enrichment in the
435 promoters of these species-specific lncRNAs (data not shown). Interestingly however, they are
436 increasingly associated with predicted expression enhancers (Supplementary Figure 10). While the
437 evolutionary and mechanistic origin of these lncRNAs is still mysterious, we could confirm that their
438 presence is associated with increased expression divergence in the neighboring genes. To test this, we
439 selected species-specific and orthologous lncRNAs that are transcribed from bidirectional promoters
440 shared with protein-coding genes, and evaluated the expression divergence of their protein-coding
441 neighbors (Supplementary Figure 9B,C). Though the difference is subtle, genes that are close to
442 species-specific lncRNAs have significantly higher expression divergence than the ones that have
443 conserved lncRNA neighbors, even after correcting for expression levels (Wilcoxon test, p-value < 10-
444 3). It thus seems that expression changes that led to the species-specific lncRNA transcription extend
445 beyond the lncRNA locus and affect the neighboring genes, as previously proposed (Kutter et al. 2012).

446 **Discussion**

447 *Assessing lncRNA functionality: current challenges and insights from evolutionary approaches*

448 More than a decade after the publication of the first genome-wide lncRNA datasets (Guttman et al.
449 2009; Khalil et al. 2009), the debate regarding their functionality is still not settled. While experimental
450 assessments of lncRNA functions are rapidly accumulating, they are lagging behind the exponential
451 increase of RNA sequencing datasets, each one revealing thousands of previously unreported
452 noncoding transcripts (Pertea et al. 2018). There is thus a need to define biologically relevant criteria
453 to prioritize lncRNAs for experimental investigation. Furthermore, *in vivo* tests of lncRNA functions
454 need to be carefully designed to account for ubiquitous confounding factors, such as the presence of

455 overlapping regulatory elements at lncRNA loci (Bassett et al. 2014). Another challenge is the fact that
456 some lncRNA loci undoubtedly have “unconventional” biological functions, that require for example
457 the presence of a transcription and splicing at a given genomic location, independently of the lncRNA
458 molecule that is produced (Latos et al. 2012; Engreitz et al. 2016).

459
460 Evolutionary approaches can provide important tools to assess biological functionality (Haerty and
461 Ponting 2014), and they have been already successfully applied to lncRNAs. Although only a few large-
462 scale comparative transcriptomics studies are available so far for vertebrate lncRNAs (Kutter et al.
463 2012; Washietl et al. 2014; Hezroni et al. 2015; Necsulea et al. 2014), they all agree that lncRNAs evolve
464 rapidly in terms of primary sequence, exon-intron structure and expression patterns, indicating that
465 there is little selective constraint and thus little functionality for these loci. However, these studies
466 have all focused on lncRNAs detected in adult organs. We hypothesized that lncRNAs expressed during
467 embryogenesis are enriched in functional loci, as suggested by the increasing number of lncRNAs with
468 proposed roles in development (Rinn et al. 2007; Sauvageau et al. 2013; Grote et al. 2013; Grote and
469 Herrmann 2015). To test this hypothesis, we performed a multi-dimensional comparative
470 transcriptomics analysis, following lncRNA and protein-coding gene expression patterns across
471 species, organs and developmental stages.

472 *Spatio-temporal lncRNA expression patterns*

473 Our first major observation is that lncRNAs are overwhelmingly detected in the adult and aged testes,
474 in agreement with previous data (Soumillon et al. 2013). Their relative depletion in embryonic and
475 newborn testes reinforces the association between lncRNA production and spermatogenesis, in accord
476 with the hypothesis that the particular chromatin environment during spermatogenesis is a driver for
477 promiscuous, non-functional transcription (Kaessmann 2010; Soumillon et al. 2013). Interestingly, we
478 show that lncRNAs are significantly differentially expressed among developmental stages, at least as
479 frequently as protein-coding genes, after correcting for their lower expression levels. However, in
480 contrast with protein-coding genes, the majority of lncRNAs reach their highest expression levels in

481 adult rather than in developing organs. As requirements for tight gene expression control are
482 undoubtedly higher during embryonic development (Ben-Tabou de-Leon and Davidson 2007), an
483 explanation for the relative lncRNA depletion in embryonic and newborn transcriptomes is that
484 transcriptional noise is more efficiently blocked during the early stages of development. Differences in
485 cellular composition heterogeneity may also be part of the explanation. Expression analyses of cell-
486 type specific markers suggest that adult and aged organ transcriptomes may be a mix of more diverse
487 cell types, notably including substantial immune cell infiltrates. A higher cell type diversity may explain
488 the increased abundance of lncRNAs in adult and aged organs, especially given that lncRNAs are
489 thought to be cell-type specific (Liu et al. 2016).

490 *Functionally constrained lncRNAs are enriched in developmental transcriptomes*

491 We show that, for those lncRNAs that are expressed above noise levels (TPM \geq 1) in somatic organs
492 and in the earlier developmental stages, there is a higher proportion of functionally constrained loci
493 than in testes-expressed lncRNAs. Strikingly, we find that the level of long-term sequence conservation
494 for lncRNA promoter regions is higher than the one observed for protein-coding promoters, when we
495 analyze genes that are robustly expressed (TPM \geq 1) in embryonic brain and kidney. Moreover, for
496 lncRNAs that are expressed in somatic organs and in the developing testes, there is significantly more
497 evolutionary constraint on promoter and splice site sequences than on exonic regions, while these
498 patterns are not seen for the bulk of lncRNAs, expressed in adult and aged testes. Thus, we show that
499 lncRNAs that are expressed in somatic organs and in the developing testes differ from those expressed
500 in the adult testes not only in terms of overall levels of sequence conservation, but also with respect
501 to the regions of the lncRNA loci that are under selective constraint. We validate previous reports of
502 increased constraint on splicing regulatory regions in mammalian lncRNAs (Schüler et al. 2014; Haerty
503 and Ponting 2015), and we show that this pattern is specifically seen in lncRNAs that are expressed in
504 somatic organs and in the developing testes. These results are also in agreement with a series of recent
505 findings, suggesting that at many lncRNA loci, biological function may reside in the presence of
506 additional non-coding regulatory elements at the lncRNA promoter rather than in the production of a

507 specific transcript (Engreitz et al. 2016; Groff et al. 2016). Thus, while there is evidence for increased
508 functionality for those lncRNA loci that are detected in developmental transcriptomes or in adult
509 somatic organs, our sequence conservation analyses suggest that their biological functions may be
510 carried out in an RNA-independent manner, as exonic sequences are under less constraint than
511 promoter or splice site regions.

512 *Evolutionary divergence of spatio-temporal expression profiles for lncRNAs*

513 We previously established that lncRNA expression patterns evolve rapidly across species in adult
514 organs. Here, we show that this rapid evolution of lncRNA expression is not restricted to adult and
515 aged individuals, but is also true for embryonic and newborn developmental stages. Expression
516 patterns comparisons across species, organs and developmental stages are dominated by differences
517 between species for lncRNAs, while similarities between organs and developmental stages are
518 predominant for protein-coding genes, even across distantly related species. We assessed the extent
519 of expression level conservation by contrasting between-species and within-species expression
520 variations and we showed that lncRNAs have significantly lower levels of conservation than protein-
521 coding genes, for all organs and developmental stages. However, lncRNA expression is significantly
522 more conserved in somatic organs and in early embryonic stages than in the adult testes. Interestingly,
523 when we evaluate expression divergence individually for each orthologous gene pair, and when we
524 correct for the lower lncRNA expression levels, we find that lncRNAs are comparable with protein-
525 coding genes, on average. Nevertheless, lncRNAs show a broader distribution of expression divergence
526 levels than protein-coding genes, and these patterns are mainly driven by species-specific expression
527 in the adult testes.

528

529 Finally, we analyzed extreme cases of expression divergence between species, namely situations
530 where transcription can be robustly detected in one species but not in the other, despite the presence
531 of good sequence conservation. We identify more than a thousand candidate species-specific lncRNAs,
532 in both mouse and rat. Interestingly, we observe that candidate mouse-specific lncRNAs are more

533 frequently transcribed from enhancers than lncRNAs conserved between mouse and rat. This
534 observation is consistent with previous reports that enhancers and enhancer-associated lncRNAs
535 evolve rapidly (Villar et al. 2015; Marques et al. 2013). The genetic basis of these extreme transcription
536 pattern changes is still not elucidated, and deserves further detailed investigations. Nevertheless, we
537 show that these lncRNA expression patterns do not occur in an isolated manner. When such species-
538 specific transcription was detected at protein-coding genes bidirectional promoters, the neighboring
539 protein-coding genes also showed increased expression divergence, compared to genes that are
540 transcribed from conserved lncRNA promoters. This observation is compatible with previous reports
541 that lncRNA turnover is associated with changes in neighboring gene expression levels (Kutter et al.
542 2012). While lncRNAs changes may be directly affecting gene expression, it is also possible that a
543 common mechanism affects both lncRNAs and protein-coding genes transcribed from bidirectional
544 promoters.

545 **Conclusions**

546 Our comparative transcriptomics approach confirms the established finding that lncRNAs repertoires,
547 sequences and expression patterns evolve rapidly across species, and shows that the accelerated rates
548 of lncRNA evolution are also seen in developmental transcriptomes. These observations are consistent
549 with the hypothesis that the majority of lncRNAs (or at least of those detected with sensitive
550 transcriptome sequencing approaches, in particular in the adult testes) may be non-functional.
551 However, we are able to modulate this conclusion, by showing that there are increased levels of
552 functional constraint on lncRNAs expressed during embryonic development, in particular in the
553 developing brain and kidney. These increased levels of constraint apply to all analyzed aspects of
554 lncRNAs, including sequence conservation for exons, promoter and splice sites, but also expression
555 pattern conservation. For many of these loci, biological function may be RNA-independent, as the
556 highest levels of selective constraint are observed on promoter regions and on splice signals, rather
557 than on lncRNA exonic sequences. Our results are thus compatible with unconventional, RNA-
558 independent functions for lncRNAs expressed during embryonic development.

560 **Methods**

561 *Biological sample collection*

562 We collected samples from three species (mouse C57BL/6J strain, rat Wistar strain and chicken White
563 Leghorn strain), four organs (brain, kidney, liver and testes) and five developmental stages (including
564 two embryonic stages, newborn, young and aged adult individuals). We sampled the following stages
565 in the mouse: embryonic day post-conception (dpc) 13.5 (E13.5 dpc, hereafter mid-stage embryo); E17
566 to E17.5 dpc (late embryo); post-natal day 1 to 2 (newborn); young adult (8-10 weeks old); aged adult
567 (24 months old). For the rat, we sampled the following stages: E15 dpc (mid-stage embryo); E18.5 to
568 E19 dpc (late embryo); post-natal day 1 to 2 (newborn); young adult (8-10 weeks old); aged adult (24
569 months, with the exception of kidney samples and two of four liver samples, derived from 12 months
570 old individuals). The embryonic and neonatal developmental stages were selected for maximum
571 comparability based on Carnegie stage criteria (Theiler 1989). For chicken, we collected samples from
572 Hamburger-Hamilton stages 31 and 36, hereafter termed mid-stage and late embryo. We selected
573 these two stages for comparability with the two embryonic stages in mouse and rat (Hamburger and
574 Hamilton 1951). In general, each sample corresponds to one individual, except for mouse and rat mid-
575 stage embryonic kidney, for which tissue from several embryos was pooled prior to RNA extraction.
576 For adult and aged organs, multiple tissue pieces from the same individual were pooled and
577 homogenized prior to RNA extraction. For brain dissection, we sampled the cerebral cortex. For mouse
578 and rat samples, with the exception of the mid-stage embryonic kidney, individuals were genotyped
579 and males were selected for RNA extraction. Between two and four biological replicates were obtained
580 for each species/organ/stage combination, amounting to 97 samples in total (Supplementary Table 1).

581 *RNA-seq library preparation and sequencing*

582 We performed RNA extractions using RNeasy Plus Mini kit from Qiagen. RNA quality was assessed
583 using the Agilent 2100 Bioanalyzer. Sequencing libraries were produced using the Illumina TruSeq

584 stranded mRNA protocol with polyA selection, and sequenced as 101 base pairs (bp) single-end reads,
585 at the Genomics Platform of iGE3 and the University of Geneva (<https://ige3.genomics.unige.ch/>).

586 Additional RNA-seq data

587 To improve detection power for lowly expressed lncRNAs, we complemented our RNA-seq collection
588 with samples generated with the same technology for Brown Norway rat adult organs (Cortez et al.
589 2014). We added data generated by the Chickspress project (<http://geneatlas.arl.arizona.edu/>) for
590 adult chicken (red jungle fowl strain UCD001) organs, as well as for embryonic chicken (White Leghorn)
591 organs from two publications (Uebbing et al. 2015; Ayers et al. 2013). Almost all samples were strand-
592 specific, except the chicken adult organs and early embryonic testes. As the data were not perfectly
593 comparable with our own in terms of library preparation and animal strains, the additional rat and
594 chicken samples were only used to increase lncRNA detection sensitivity.

595 RNA-seq data processing

596 We used HISAT2 (Kim et al. 2015) release 2.0.5 to align the RNA-seq data on reference genomes. The
597 genome sequences (assembly versions mm10/GRCm38, rn6/Rnor_6.0 and galGal5/Gallus_gallus-5.0)
598 were downloaded from the Ensembl database (Cunningham et al. 2019). Genome indexes were built
599 using only genome sequence information. To improve detection sensitivity, at the alignment step we
600 provided known splice junction coordinates extracted from Ensembl. We set the maximum intron
601 length for splice junction detection at 1 million base pairs (Mb). To verify the strandedness of the RNA-
602 seq data, we analyzed spliced reads that spanned introns with canonical (GT-AG or GC-AG) splice sites
603 and compared the strand inferred based on the splice site with the one assigned based on the library
604 preparation protocol (Supplementary Table 1). Finally, to estimate the mappability of each genomic
605 region, we generated error-free artificial RNA-seq reads (single-end, 101 bp long, with 5 bp distance
606 between consecutive read starts) from the genome sequence and realigned them to the genome with
607 the same HISAT2 parameters. Regions for which the corresponding reads could be aligned
608 unambiguously were considered “mappable”; the remaining regions were said to be “unmappable”.

609 Transcript assembly and filtering

610 We assembled transcripts for each sample using StringTie (Pertea et al. 2015), release 1.3.5, based on
611 read alignments obtained with HISAT2. We provided genome annotations from Ensembl release 94 as
612 a guide for transcript assembly. We filtered Ensembl annotations to remove transcripts that spanned
613 a genomic length above 2.5 Mb. For protein-coding genes, we kept only protein-coding transcripts,
614 discarding isoforms annotated as “retained_intron”, “processed_transcript” etc. We set the minimum
615 exonic length at 150 bp, the minimum anchor length for splice junctions at 8bp and the minimum
616 isoform fraction at 0.05. We compared the resulting assembled transcripts with Ensembl annotations
617 and we discarded read-through transcripts, defined as overlapping with multiple multi-exonic
618 Ensembl-annotated genes. For strand-specific samples, we discarded transcripts for which the ratio of
619 sense to antisense unique read coverage was below 0.01. We discarded multi-exonic transcripts that
620 were not supported by splice junctions with correctly assigned strands. The filtered transcripts
621 obtained for each sample were assembled into a single dataset *per* species using the merge option in
622 StringTie. For increased sensitivity, we removed the minimum FPKM and TPM thresholds for transcript
623 inclusion. We constructed a combined annotation dataset, starting with Ensembl annotations, to
624 which we added newly-assembled transcripts that had no exonic overlap with Ensembl genes. We also
625 included newly-annotated isoforms for known genes if they had exonic overlap with exactly one
626 Ensembl gene, thus discarding potential read-through transcripts or gene fusions.

627 Protein-coding potential of assembled transcripts

628 To determine whether the newly assembled transcripts were protein-coding or non-coding, we mainly
629 relied on the codon substitution frequency (CSF) score (Lin et al. 2007). As in a previous publication
630 (Necsulea et al. 2014) we scanned whole genome alignments and computed CSF scores in 75 bp sliding
631 windows moving with a 3 bp step. We used pre-computed alignments downloaded from the UCSC
632 Genome Browser (Casper et al. 2018), including the alignment between the mouse genome and 59
633 other vertebrates (for mouse classification), between the human genome and 99 other vertebrates

634 (for rat and chicken classification) and between the rat genome and 19 other vertebrates (for rat
635 classification). For each window, we computed the score in each of the 6 possible reading frames and
636 extracted the maximum score for each strand. We considered that transcripts are protein-coding if
637 they overlapped with positive CSF scores on at least 150 bp. As positive CSF scores may also appear on
638 the antisense strand of protein-coding regions due to the partial strand-symmetry of the genetic code,
639 in this analysis we considered only exonic regions that did not overlap with other genes. In addition,
640 we searched for sequence similarity between assembled transcripts and known protein sequences
641 from the SwissProt 2017_04 (The UniProt Consortium 2017) and Pfam 31.0 (El-Gebali et al. 2019)
642 databases. We kept only SwissProt entries with confidence scores 1, 2 or 3 and we used the Pfam-A
643 curated section of Pfam. We searched for sequence similarity using the blastx utility in the BLAST+
644 2.8.1 package (Camacho et al. 2009; Altschul et al. 1990), keeping hits with maximum e-value 1e-3 and
645 minimum protein sequence identity 40%, on repeat-masked cDNA sequences. We considered that
646 transcripts were protein-coding if they overlapped with blastx hits over at least 150 bp. Genes were
647 said to be protein-coding if at least one of their isoforms was classified as protein-coding, based on
648 either the CSF score or on sequence similarity with known proteins.

649 Long non-coding RNA selection

650 To construct a reliable lncRNA dataset, we selected newly-annotated genes classified as non-coding
651 based on both the CSF score and on sequence similarity with known proteins and protein domains, as
652 well as Ensembl-annotated genes with non-coding biotypes ("lincRNA", "processed_transcript",
653 "antisense", "TEC", "macro_lincRNA", "bidirectional_promoter_lincRNA", "sense_intronic"). For newly
654 detected genes, we applied several additional filters: we required a minimum exonic length
655 (corresponding to the union of all annotated isoforms) of at least 200 bp for multi-exonic loci and of
656 at least 500 bp for mono-exonic loci; we eliminated genes that overlapped for more than 5% of their
657 exonic length with unmappable regions; we kept only loci that were classified as intergenic and at least
658 5 kb away from Ensembl-annotated protein-coding genes on the same strand; for multi-exonic loci, we
659 required that all splice junctions be supported by reads with correct strand assignment (cf. above). For

660 both *de novo* and Ensembl annotations, we removed transcribed loci that overlapped on at least 50%
661 of their length with retrotransposed gene copies, annotated by the UCSC Genome Browser and from
662 a previous publication (Carelli et al. 2016); we discarded loci that overlapped with UCSC-annotated
663 tRNA genes and with RNA-type elements from RepeatMasker (Smit et al. 2003) on at least 25% of their
664 length. We kept loci supported by at least 10 uniquely mapped RNA-seq reads and for which a ratio of
665 sense to antisense transcription of at least 1% was observed in at least one sample.

666 Gene expression estimation

667 We computed the number of uniquely mapping reads unambiguously attributed to each gene using
668 the Rsubread package in R (Liao et al. 2019), discarding reads that overlapped with multiple genes. We
669 also estimated read counts and TPM (transcript *per* million) values *per* gene using Kallisto (Bray et al.
670 2016). To approach absolute expression levels estimates, for better comparisons across samples, we
671 further normalized TPM values using a scaling approach (Brawand et al. 2011). Briefly, we ranked the
672 genes in each sample according to their TPM values, we computed the variance of the ranks across all
673 samples for each gene, and we identified the 100 least-varying genes, found within the inter-quartile
674 range (25%-75%) in terms of average expression levels across samples. We derived normalization
675 coefficients for each sample such that the median of the 100 least-varying genes be identical across
676 samples. We then used these coefficients to normalize TPM values for each sample. We excluded
677 mitochondrial genes from expression estimations and analyses, as these genes are highly expressed
678 and can be variable across samples.

679 Differential expression analyses

680 We used the DESeq2 (Love et al. 2014)(Smedley et al. 2009)(74)(75) package release 1.22.2 in R release
681 3.5.0 (R Core Team 2018) to test for differential expression across developmental stages, separately
682 for each organ and species. We analyzed both protein-coding genes and lncRNAs, selected according
683 to the criteria described above. We first performed a global differential expression analysis, using the
684 likelihood ratio test to contrast a model including an effect of the developmental stage against the null

685 hypothesis of homogeneous expression level across all developmental stages. This analysis was
686 performed on all annotated protein-coding and lncRNA genes for each species, as well as on 1-to-1
687 orthologous genes for mouse and rat. In addition, we down-sampled the numbers of reads assigned
688 to protein-coding genes to obtain identical average numbers of reads for protein-coding genes and
689 lncRNAs. We also contrasted consecutive developmental stages, for each species and organ. For each
690 test, we also computed the expression fold change based on average TPM values for each
691 developmental stage/organ combination.

692 Expression specificity index

693 We used the previously proposed tissue specificity index (Liao et al. 2006) to measure gene expression
694 specificity across organs and developmental stages, provided by the formula: $\tau = \sum (1 - r_i)/(n-1)$,
695 where r_i represents the ratio between the expression level in sample i and the maximum expression
696 level across samples, and n represents the total number of samples. We computed this index on
697 normalized TPM values, averaged across all replicates for a given species / organ / developmental stage
698 combination (Supplementary Dataset 3).

699 Homologous lncRNA family prediction

700 We used existing whole-genome alignments as a guide to predict homologous lncRNAs across species,
701 as previously proposed (Washietl et al. 2014). We first constructed for each gene the union of its exon
702 coordinates across all isoforms, hereafter termed “exon blocks”. We projected exon block coordinates
703 between pairs of species using the liftOver utility and whole-genome alignments generated with blastz
704 (http://www.bx.psu.edu/miller_lab/), available through the UCSC Genome Browser (Casper et al.
705 2018). To increase detection sensitivity, for the initial liftOver projection we required only that 10% of
706 the reference bases remap on the target genome. Projections were then filtered, retaining only cases
707 where the size ratio between the projected and the reference region was between 0.33 and 3 for
708 mouse and rat (0.2 and 5 for comparisons involving chicken). To exclude recent lineage-specific
709 duplications, regions with ambiguous or split liftOver projections were discarded. For genes where

710 multiple exon blocks could be projected across species, we defined the consensus chromosome and
711 strand in the target genome and discarded projected exon blocks that did not match this consensus.
712 We then evaluated the order of the projected exon blocks on the target genes, to identify potential
713 internal rearrangements. If internal rearrangements were due to the position of a single projected
714 exon block, the conflicting exon block was discarded; otherwise, the entire projected gene was
715 eliminated. As the projected reference gene coordinates could overlap with multiple genes in the
716 target genome, we constructed gene clusters based on the overlap between projected exon block
717 coordinates and target annotations, using a single-link clustering approach. We then realigned entire
718 genomic loci for each pair of reference-target genes found within a cluster, using lastz
719 (http://www.bx.psu.edu/miller_lab/) and the threaded blockset aligner (Blanchette et al. 2004). Using
720 this alignment, we computed the percentage of exonic sequences aligned without gaps and the
721 percentage of identical exonic sequence, for each pair of reference-target genes. We then extracted
722 the best hit in the target genome for each gene in the reference genome based on the percentage of
723 identical exonic sequence, requiring that the ratio between the maximum percent identity and the
724 percent identity of the second-best hit be above 1.1. Reciprocal best hits were considered to be 1-to-
725 1 orthologous loci between pairs of species. For analyses across all three species, we constructed
726 clusters of reciprocal best hits from pairwise species comparisons, using a single-link clustering
727 approach. Resulting clusters with more than 1 representative *per* species were discarded. To examine
728 the validity of our procedure for homologous gene family prediction, we compared the resulting gene
729 families with predictions from the Ensembl Compara pipeline (Herrero et al. 2016), extracted from
730 Ensembl release 94, for protein-coding genes.

731 Sequence evolution

732 We evaluated long-term evolutionary sequence conservation based on PhastCons (Siepel et al. 2005)
733 scores, computed for the mouse genome using either a placental mammal or a vertebrate multiple
734 species alignment available from the UCSC Genome Browser (Casper et al. 2018). We computed
735 average PhastCons scores on exonic sequences (excluding exonic regions overlapping with other

736 genes), promoter regions (defined as 1 kb immediately upstream of the transcription start site) and
737 splice sites (defined as the first two and last two bases of each intron). For genes with multiple
738 promoters, we computed the average score across all promoters.

739 Gene expression evolution

740 We computed global and *per*-gene expression level conservation between mouse and rat, for 1-to-1
741 orthologous genes. We first measured gene expression conservation for protein-coding genes and
742 lncRNAs as a class. For each organ/developmental stage, we computed the expression level correlation
743 between mouse and rat average TPM levels, across all orthologous pairs. We also computed the
744 correlation between individuals within the same species; for organ/stages with more than two
745 biological replicates we computed the average correlation coefficient across all possible pairs of
746 individuals. We then evaluated the global extent of gene expression conservation through the ratio of
747 the between-species correlation coefficient to the average within-species correlation coefficient.
748 Spearman's rank correlation coefficients were used in all cases. We obtained 95% confidence intervals
749 for expression conservation measures through a bootstrap procedure, resampling 100 times the same
750 number of genes with replacement. In addition to this global measure of expression conservation, we
751 estimated the extent of between-species expression divergence *per* gene by computing Euclidean
752 distances between relative expression profiles for each species. The relative expression profiles were
753 derived from TPM values *per* organ/developmental stage, averaged across biological replicates,
754 divided by the sum of all average TPM values.

755 Statistical analyses and graphical representations

756 All statistical analyses and graphical representations were done with R (R Core Team 2018), version
757 3.5.0. We performed principal component analyses using the *ade4* library (Dray and Dufour 2007) and
758 hierarchical clustering of gene expression matrices using the *hclust* function in the *stats* package in R,
759 on pairwise Euclidean distances. For all analyses involving multiple statistical tests, false discovery
760 rates were computed with the Benjamini-Hochberg procedure (Benjamini and Hochberg 1995). 95%

761 confidence intervals for median values of distributions were computed with the following formula:
762 median +/- 1.57 x IQR/sqrt(N), where IQR is the inter-quartile range, sqrt denotes the square root and
763 N the number of points.

764 **Availability of data and materials**

765 The raw and processed RNA-seq data were submitted to the NCBI Gene Expression Omnibus (GEO),
766 under accession number GSE108348. Additional processed files and all scripts used to analyze the
767 data are available at the address: ftp://pbil.univ-lyon1.fr/pub/datasets/Darbellay_LncEvoDevo.

768

769 **Author contributions**

770 FD performed organ dissections, RNA extractions, quality control, prepared samples for sequencing
771 and contributed to study design and manuscript preparation. AN designed the study, performed
772 computational analyses and wrote the manuscript. All authors read and approved the final manuscript.

773 **Acknowledgements**

774 We thank Denis Duboule and all members of the laboratory for advice and support, Mylene Docquier,
775 Brice Petit and the Genomics Platform of the University of Geneva for RNA-seq data production,
776 Amanda Cooksey and the Chickspress Team at the University of Arizona
777 (<http://geneatlas.arl.arizona.edu>) for granting us access to chicken RNA-seq data, Ioannis Xenarios and
778 the Vital-IT team for computational support. We thank Jean-Marc Matter (University of Geneva) for
779 providing chicken eggs. This work was performed using the computing facilities of the CC LBBE/PRABI,
780 the Vital-IT Center for high-performance computing of the SIB Swiss Institute of Bioinformatics
781 (<http://www.vital-it.ch>) and the computing center of the French National Institute of Nuclear and
782 Particle Physics (CC-IN2P3). This project was funded by the Swiss National Science Foundation (SNSF
783 Ambizione grant PZ00P3_142636), the Agence Nationale pour la Recherche (ANR JCJC 2017
784 LncEvoSys). FD was supported by a FP7 IDEAL grant (259679).

785

786 **Figure legends**

787 **Figure 1. Transcriptome complexity across organs and developmental stages.**

788 **A.** Experimental design. The developmental stages selected for mouse, rat and chicken are marked on
789 a horizontal axis. Organs sampled for each species and developmental stage are shown below.
790 Abbreviations: br, brain; kd, kidney; lv, liver; ts, testes.

791 **B.** Expression of cell type-specific markers derived from single-cell experiments (full list provided in
792 Supplementary Table 3), in our mouse and rat RNA-seq samples. The heatmap represents centered
793 and scaled log₂-transformed TPM levels (z-score). Developmental stages are indicated by numeric
794 labels, 1 to 5. Average levels across biological replicates are shown. Species are color-coded, shown
795 below the heatmap.

796 **C.** Number of protein-coding genes supported by at least 10 uniquely mapped reads in each sample,
797 after read resampling to homogenize coverage (Methods).

798 **D.** Number of lncRNAs supported by at least 10 uniquely mapped reads in each sample, after read
799 resampling to homogenize coverage.

800

801 **Figure 2. Protein-coding gene expression is conserved across organs and developmental stages.**

802 **A.** First factorial map of a principal component analysis, performed on log₂-transformed TPM values,
803 for 10,363 protein-coding genes with orthologues in mouse, rat and chicken. Colors represent different
804 organs and developmental stages, point shapes represent different species.

805 **B.** Hierarchical clustering, performed on a distance matrix derived from Spearman correlations
806 between pairs of samples, for 10,363 protein-coding genes with orthologues in mouse, rat and chicken.
807 Organ and developmental stages are color-coded, shown below the heatmap. Species of origin is color-
808 coded, shown on the right. Sample clustering is shown on the left.

809 **C.** Expression profiles of protein-coding genes that are significantly differentially expressed (FDR<0.01)
810 among developmental stages, for both mouse and rat, in the brain. TPM values were averaged across
811 replicates and normalized by dividing by the maximum value, for each species. The resulting relative

812 expression profiles were combined across species and clustered with the K-means algorithm. The
813 average profiles of the genes belonging to each cluster are shown. Gray lines represent profiles of
814 individual genes from a cluster.

815

816 **Figure 3. Different expression patterns for protein-coding genes and lncRNAs.**

817 **A.** Distribution of the organ in which maximum expression is observed, for protein-coding genes (pc)
818 and lncRNAs (lnc), for mouse, rat and chicken. Organs are color-coded, shown above the plot.

819 **B.** Distribution of the developmental stage in which maximum expression is observed, for protein-
820 coding genes and lncRNAs, for mouse, rat and chicken. Developmental stages are color-coded, shown
821 above the plot.

822 **C.** Percentage of protein-coding and lncRNA genes that are significantly ($FDR < 0.01$) DE among
823 developmental stages, with respect to the total number of genes tested for each organ. Left panel:
824 differential expression analysis performed with all RNA-seq reads. Right panel: differential expression
825 analysis performed after down-sampling read counts for protein-coding genes, to match those of
826 lncRNAs (Methods).

827 **D.** Distribution of the developmental stage in which maximum expression is observed, for protein-
828 coding genes and lncRNAs that are significantly DE ($FDR < 0.01$) in each organ, for the mouse. The
829 percentages are computed with respect to the total number of DE genes in each organ and each gene
830 class.

831

832 **Figure 4. Increased levels of long-term sequence conservation for lncRNAs expressed early in**
833 **development.**

834 **A.** Distribution of the PhastCons sequence conservation score for protein-coding and lncRNAs exonic
835 regions, for subsets of genes expressed above noise levels ($TPM \geq 1$) in each organ and developmental
836 stage. We used precomputed PhastCons score for placental mammals, downloaded from the UCSC
837 Genome Browser. Exonic regions that overlap with exons from other genes were masked. Dots

838 represent median values, vertical bars represent 95% confidence intervals. Numbers of analyzed genes
839 are provided in Supplementary Table 4.

840 **B.** Same as A, for promoter regions (1kb upstream of transcription start sites). Exonic sequences were
841 masked before assessing conservation.

842 **C.** Same as B, for splice sites (first and last two bases of each intron).

843

844 **Figure 5. Orthologous lncRNA families for mouse, rat and chicken.**

845 **A.** Number of mouse protein-coding genes and lncRNAs in different classes of evolutionary
846 conservation. From left to right: all loci (with TPM \geq 1 in at least one mouse sample), loci with
847 conserved sequence in the rat, loci for which transcription could be detected (at least 10 unique reads)
848 in predicted orthologous locus in the rat, loci with predicted 1-to-1 orthologues, loci for which the
849 predicted orthologue belonged to the same class (protein-coding or lncRNA) in the rat, loci with
850 conserved sequence in the chicken, loci for which transcription could be detected (at least 10 unique
851 reads) in predicted orthologous locus in the chicken, loci with predicted 1-to-1 orthologues, loci for
852 which the predicted orthologue belonged to the same class (protein-coding or lncRNA) in the chicken.
853 We analyze 17,868 protein-coding genes and 12,199 candidate lncRNAs with an expression level (TPM)
854 \geq 1 in at least one mouse sample.

855 **B.** Distribution of the organ in which maximum expression is observed, for mouse protein-coding and
856 lncRNA genes that have no orthologues in the rat or chicken, for genes with orthologues in the rat and
857 for genes with orthologues in chicken.

858 **C.** Same as B, for the distribution of the developmental stage in which maximum expression is
859 observed.

860

861 **Figure 6. Global comparison of lncRNA expression patterns across species.**

862 **A.** First factorial map of a principal component analysis, performed on log₂-transformed TPM values,
863 for 2,754 orthologous mouse and rat lncRNAs expressed above noise levels (TPM \geq 1) in at least one

864 mouse or rat sample. Colors represent different organs and developmental stages, point types
865 represent species.

866 **B.** Hierarchical clustering, performed on a distance matrix derived from Spearman correlations
867 between pairs of samples, for 2,754 orthologous mouse and rat lncRNAs. Organ and developmental
868 stages are shown below the heatmap. Species of origin is shown on the right. Sample clustering is
869 shown on the left.

870

871 **Figure 7. Global estimates of expression conservation across organs and developmental stages.**

872 **A.** Example of between-species and within-species variation of expression levels, for protein-coding
873 genes (left) and lncRNAs (right), for orthologous genes between mouse and rat, for the mid-stage
874 embryonic brain. Spearman's correlation coefficients (ρ) are shown above each plot. We show a
875 smoothed color density representation of the scatterplots, obtained through a (2D) kernel density
876 estimate (smoothScatter function in R).

877 **B.** Expression conservation index, defined as the ratio of the between-species and the within-species
878 expression level correlation coefficients, for protein-coding genes, for each organ and developmental
879 stage. The vertical segments represent minimum and maximum values obtained from 100 bootstrap
880 replicates. We analyzed 14,919 pairs of orthologous genes between mouse and rat, with TPM ≥ 1 in
881 at least one sample.

882 **C.** Same as B, for lncRNAs. We analyzed 2,754 orthologous mouse and rat lncRNAs with TPM ≥ 1 in at
883 least one mouse or rat sample.

884

885 **Figure 8. Per-gene estimates of expression pattern divergence between species.**

886 **A.** Relationship between the per-gene expression divergence measure (Euclidean distance of relative
887 expression profiles among organs/stages, between mouse and rat), and the average expression values
888 (\log_2 -transformed TPM) across all mouse and rat samples. We show a smoothed color density

889 representation of the scatterplots, obtained through a (2D) kernel density estimate (smoothScatter
890 function in R). Red line: linear regression.

891 **B.** Distribution of the expression divergence value for all protein-coding and lncRNA genes with
892 predicted 1-to-1 orthologues in mouse and rat.

893 **C.** Distribution of the residual expression divergence values, after regressing the average expression
894 level, for protein-coding genes and lncRNAs.

895 **D.** Relationship between expression divergence and exonic sequence conservation (% exonic sequence
896 aligned without gaps between mouse and rat), for protein-coding genes and lncRNAs.

897 **E.** Average contribution of each organ/developmental stage combination to expression divergence, for
898 protein-coding genes and lncRNAs.

899

900 **Supplementary Figure 1. Expression patterns of cell-type specific markers in mouse, rat and chicken**
901 **samples.**

902 **A.** Expression of cell type-specific markers derived from single-cell experiments (full list provided in
903 Supplementary Table 3), in our mouse, rat and chicken RNA-seq samples. The heatmap represents
904 centered and scaled log₂-transformed TPM levels (z-score). Developmental stages are indicated by
905 numeric labels, 1 to 5. Average levels across biological replicates are shown. We show only organs and
906 developmental stages that were sampled in all three species, for genes with 1-to-1 orthologues.

907

908 **Supplementary Figure 2. Conservation of developmental expression profiles between mouse and**
909 **rat, for protein-coding genes.**

910 **A.** Expression profiles of orthologous protein-coding genes that are significantly differentially
911 expressed (FDR<0.01) among developmental stages, for both mouse and rat, in the kidney. TPM values
912 were averaged across replicates and normalized by dividing by the maximum, for each species. The
913 resulting relative expression profiles were combined across species and clustered with the K-means

914 algorithm. The average profiles of the genes belonging to each cluster are shown. Gray lines represent
915 profiles of individual genes from a cluster. Numbers of genes in each cluster are shown in the plot.

916 **B.** Same as A, for the liver.

917 **C.** Same as A, for the testes. For this organ, we searched for only 4 clusters with the K-means algorithm.

918

919 **Supplementary Figure 3. Protein-coding genes and lncRNA expression patterns.**

920 **A.** Distribution of the maximum expression level (log₂-transformed TPM values), for protein-coding
921 genes (red) and lncRNAs (blue), for mouse, rat and chicken. We show only genes that are expressed
922 above noise levels (TPM \geq 1) in at least one sample.

923 **B.** Distribution of the expression specificity index (Methods) for protein-coding genes and lncRNAs, in
924 the mouse. Genes were divided into 5 expression bins, based on their maximum expression level across
925 samples.

926 **C.** Same as B, for the rat.

927 **D.** Distribution of the ratio between the minimum and the maximum TPM value across developmental
928 stages, for genes that are significantly differentially expressed among stages for each organ and
929 species. Lower values indicate stronger expression changes among developmental stages.

930 **E.** Distribution of the developmental stage in which maximum expression is observed, for protein-
931 coding genes and lncRNAs that are significantly DE (FDR $<$ 0.01) in each organ, for the rat. The
932 percentages are computed with respect to the total number of DE genes in each organ and each gene
933 class.

934

935 **Supplementary Figure 4. Estimates of long-term sequence conservation scores for different regions
936 of lncRNAs loci.**

937 **A.** Distribution of the difference between the exonic PhastCons score and the promoter PhastCons
938 score, for mouse lncRNAs that are expressed above noise levels (TPM \geq 1) in each organ and
939 developmental stage. Precomputed PhastCons score for placental mammals were provided by the

940 UCSC Genome Browser. Exonic regions that overlap with other genes were masked. Dots represent
941 median values, vertical bars represent 95% confidence intervals. Numbers of analyzed genes are
942 provided in Supplementary Table 4.

943 **B.** Same as A, for the difference between exonic and splice site PhastCons score.

944 **C.** Distribution of the promoter sequence conservation score, for all lncRNAs, for lncRNAs that have
945 bidirectional promoters and for lncRNAs that overlap with Encode-annotated enhancers, in the mouse.

946

947 **Supplementary Figure 5. Expression patterns of 30 lncRNAs conserved in mouse, rat and chicken.**

948 **A.** Heatmap of the centered and scaled expression values (log₂-transformed TPM), for 30 lncRNAs that
949 are shared across mouse, rat and chicken. For comparability with chicken, we show only mid-stage and
950 late embryo samples for mouse and rat, for somatic organs. The annotation source is shown on the
951 right: gray rectangles indicate a newly-annotated gene. Organs and developmental stages are depicted
952 by color rectangles below the heatmap. The list of genes used for this analysis is provided in
953 Supplementary Table 6.

954

955 **Supplementary Figure 6. Main sources of expression pattern variability for protein-coding genes and**
956 **lncRNAs.**

957 **A.** Coordinates on the first five axes of the principal component analysis, for mouse and rat orthologous
958 protein-coding genes. Points represent individual samples. Organs are color-coded and developmental
959 stages are distinguished by point types. Mouse (m, filled dots) and rat (r, unfilled dots) samples are
960 shown on separate x-axis positions.

961 **B.** Same as A, for lncRNAs.

962

963 **Supplementary Figure 7. Conservation of developmental expression profiles between mouse and**
964 **rat, for lncRNAs.**

965 **A.** Expression patterns of orthologous lncRNAs that are significantly differentially expressed
966 (FDR<0.01) among developmental stages, for both mouse and rat, in the brain. TPM values were
967 averaged across replicates and normalized by dividing by the maximum value for each species. The
968 resulting relative expression profiles were combined across species and clustered with the K-means
969 algorithm. The average profiles of the genes belonging to each cluster are shown. Gray lines represent
970 profiles of individual genes from a cluster.

971 **B.** Same as A, for the kidney.

972 **C.** Same as A, for the liver.

973 **D.** Same as A, for the testes. For this organ, we searched for only 4 clusters with the K-means algorithm.

974

975 **Supplementary Figure 8. Examples of genes with high expression pattern divergence between**
976 **mouse and rat.**

977 **A.** Examples of average expression profile in mouse and rat, for the top 2 most-divergent protein-
978 coding and lncRNA genes.

979

980 **Supplementary Figure 9. Candidate species-specific lncRNAs.**

981 **A.** Genomic localization and RNA-seq read coverage of a candidate mouse-specific lncRNA, situated
982 downstream of the *Fzd4* gene. RNA-seq data is shown for young and aged adult kidney.

983 **B.** Distribution of the raw expression divergence for protein-coding genes that are transcribed from
984 the same bidirectional promoters as lncRNAs with 1-to-1 orthologues in mouse and rat (black), or as
985 candidate species-specific lncRNAs (red).

986 **C.** Same as A, after correcting for the average expression level of the protein-coding genes.

987

988 **Supplementary Figure 10. Genomic and expression characteristics of candidate species-specific**
989 **lncRNAs.**

990 **A.** Percentage of mouse lncRNAs for which the predicted transcription start site is found within 1kb
991 of an Encode-annotated enhancer. lncRNAs are divided into loci with predicted 1-to-1 orthologues in
992 the rat (1-1, dark blue) and mouse-specific lncRNAs (light blue). lncRNAs are further separated into
993 newly-annotated (new) or previously known (Ensembl).

994 **B.** Same as A, for the percentage of multi-exonic loci, for mouse and rat.

995 **C.** Same as A, for the percentage of loci that have predicted bidirectional promoters, for mouse and
996 rat.

997 **D.** Distribution of the organ in which maximum expression is observed, for mouse and rat lncRNAs.
998 lncRNAs are divided into loci with predicted 1-to-1 orthologues (1-1) and species-specific lncRNAs (sp).

999 **E.** Same as D, for the distribution of the developmental stage in which maximum expression is
1000 observed.

1001

1002 **Supplementary Table List.**

1003 **Supplementary Table 1.** List of RNA-seq samples generated specifically for this project, and used for
1004 all downstream expression analyses.

1005 **Supplementary Table 2.** List of additional, previously published RNA-seq samples, included in the
1006 lncRNA detection pipeline.

1007 **Supplementary Table 3.** Cell-type markers for the four organs analyzed here, derived from single-cell
1008 transcriptomics analyses.

1009 **Supplementary Table 4.** Numbers of protein-coding genes and lncRNAs that have an average TPM
1010 expression level of at least 1 in each organ / developmental stage combination, for each species.

1011 **Supplementary Table 5.** Sequence conservation scores (average PhastCons scores), for exons, introns,
1012 promoters and splice sites, for mouse protein-coding genes and lncRNAs.

1013 **Supplementary Table 6.** List of 30 lncRNAs that are predicted to be 1-to-1 orthologues in mouse, rat
1014 and chicken.

1015 **Supplementary Table 7.** Expression pattern and sequence conservation scores for protein-coding
1016 genes and lncRNAs, for mouse and rat 1-to-1 orthologues.

1017

1018 **Supplementary Dataset List.**

1019 **Supplementary Dataset 1.** Complete gene annotations for mouse, rat and chicken.

1020 **Supplementary Dataset 2.** Gene expression levels (raw and normalized TPM values, unique read
1021 counts).

1022 **Supplementary Dataset 3.** Expression patterns (average across replicates, samples with maximum
1023 expression) and expression specificity indexes.

1024 **Supplementary Dataset 4.** Results of the differential expression analyses across all developmental
1025 stages, or between consecutive developmental stages, for each organ and each species.

1026 **Supplementary Dataset 5.** Predicted orthologous gene families and sequence conservation statistics.

1027 **Supplementary Dataset 6.** Raw and normalized expression values (TPM) for orthologous protein-
1028 coding and lncRNA families.

1029 **Supplementary Dataset 7.** Expression pattern divergence for mouse and rat orthologous genes.

1030 **Supplementary Dataset 8.** Lists of candidate species-specific lncRNAs.

1031

1032

1033 **References**

- 1034 Altschul SF, Gish W, Miller W, Myers EW, Lipman DJ. 1990. Basic local alignment search tool. *J Mol Biol*
1035 **215**: 403–410.
- 1036 Amândio AR, Necsulea A, Joye E, Mascrez B, Duboule D. 2016. Hotair is dispensible for mouse
1037 development. *PLoS Genet* **12**: e1006232.
- 1038 Anders S, Huber W. 2010. Differential expression analysis for sequence count data. *Genome Biol* **11**:
1039 R106.
- 1040 Anderson KM, Anderson DM, McAnally JR, Shelton JM, Bassel-Duby R, Olson EN. 2016. Transcription
1041 of the non-coding RNA upperhand controls Hand2 expression and heart development. *Nature*
1042 **539**: 433–436.
- 1043 Arendt D, Musser JM, Baker CVH, Bergman A, Cepko C, Erwin DH, Pavlicev M, Schlosser G, Widder S,
1044 Laubichler MD, et al. 2016. The origin and evolution of cell types. *Nat Rev Genet* **17**: 744–757.
- 1045 Ayers KL, Davidson NM, Demiyah D, Roeszler KN, Grützner F, Sinclair AH, Oshlack A, Smith CA. 2013.
1046 RNA sequencing reveals sexually dimorphic gene expression before gonadal differentiation in
1047 chicken and allows comprehensive annotation of the W-chromosome. *Genome Biol* **14**.
- 1048 Bassett AR, Akhtar A, Barlow DP, Bird AP, Brockdorff N, Duboule D, Ephrussi A, Ferguson-Smith AC,
1049 Gingeras TR, Haerty W, et al. 2014. Considerations when investigating lncRNA function in vivo.
1050 *eLife* **3**: e03058.
- 1051 Benjamini Y, Hochberg Y. 1995. Controlling the false discovery rate: a practical and powerful approach
1052 to multiple testing. *J Roy Stat Soc B* **57**: 289+300.
- 1053 Ben-Tabou de-Leon S, Davidson EH. 2007. Gene regulation: gene control network in development.
1054 *Annu Rev Biophys Biomol Struct* **36**: 191.
- 1055 Blanchette M, Kent WJ, Riemer C, Elnitski L, Smit AFA, Roskin KM, Baertsch R, Rosenbloom K, Clawson
1056 H, Green ED, et al. 2004. Aligning multiple genomic sequences with the threaded blockset
1057 aligner. *Genome Res* **14**: 708–715.
- 1058 Brannan CI, Dees EC, Ingram RS, Tilghman SM. 1990. The product of the H19 gene may function as an
1059 RNA. *Mol Cell Biol* **10**: 28–36.
- 1060 Brawand D, Soumillon M, Necsulea A, Julien P, Csárdi G, Harrigan P, Weier M, Liechti A, Aximu-Petri A,
1061 Kircher M, et al. 2011. The evolution of gene expression levels in mammalian organs. *Nature*
1062 **478**: 343–348.
- 1063 Bray NL, Pimentel H, Melsted P, Pachter L. 2016. Near-optimal probabilistic RNA-seq quantification.
1064 *Nat Biotechnol* **34**: 525–527.
- 1065 Brown CJ, Ballabio A, Rupert JL, Lafreniere RG, Grompe M, Tonlorenzi R, Willard HF. 1991. A gene from
1066 the region of the human X inactivation centre is expressed exclusively from the inactive X
1067 chromosome. *Nature* **349**: 38–44.
- 1068 Camacho C, Coulouris G, Avagyan V, Ma N, Papadopoulos J, Bealer K, Madden TL. 2009. BLAST+:
1069 architecture and applications. *BMC Bioinformatics* **10**: 421.

- 1070 Carelli FN, Hayakawa T, Go Y, Imai H, Warnefors M, Kaessmann H. 2016. The life history of retrocopies
1071 illuminates the evolution of new mammalian genes. *Genome Res* **26**: 301–314.
- 1072 Casper J, Zweig AS, Villarreal C, Tyner C, Speir ML, Rosenbloom KR, Raney BJ, Lee CM, Lee BT, Karolchik
1073 D, et al. 2018. The UCSC Genome Browser database: 2018 update. *Nucleic Acids Res* **46**: D762–
1074 D769.
- 1075 Cesana M, Cacchiarelli D, Legnini I, Santini T, Sthandier O, Chinappi M, Tramontano A, Bozzoni I. 2011.
1076 A long noncoding RNA controls muscle differentiation by functioning as a competing
1077 endogenous RNA. *Cell* **147**: 358–369.
- 1078 Cortez D, Marin R, Toledo-Flores D, Froidevaux L, Liechti A, Waters PD, Grützner F, Kaessmann H. 2014.
1079 Origins and functional evolution of Y chromosomes across mammals. *Nature* **508**: 488–93.
- 1080 Cunningham F, Achuthan P, Akanni W, Allen J, Amode MR, Armean IM, Bennett R, Bhai J, Billis K, Boddu
1081 S, et al. 2019. Ensembl 2019. *Nucleic Acids Res* **47**: D745–D751.
- 1082 Doolittle WF. 2018. We simply cannot go on being so vague about “function.” *Genome Biol* **19**: 223.
- 1083 Dray S, Dufour AB. 2007. The ade4 package: implementing the duality diagram for ecologists. *J Stat*
1084 *Softw* **22**: 1–20.
- 1085 El-Gebali S, Mistry J, Bateman A, Eddy SR, Luciani A, Potter SC, Qureshi M, Richardson LJ, Salazar GA,
1086 Smart A, et al. 2019. The Pfam protein families database in 2019. *Nucleic Acids Res* **47**: D427–
1087 D432.
- 1088 Engreitz JM, Haines JE, Perez EM, Munson G, Chen J, Kane M, McDonel PE, Guttman M, Lander ES.
1089 2016. Local regulation of gene expression by lncRNA promoters, transcription and splicing.
1090 *Nature* **539**: 452–455.
- 1091 Gendrel A-V, Heard E. 2014. Noncoding RNAs and epigenetic mechanisms during X-chromosome
1092 inactivation. *Annu Rev Cell Dev Biol* **30**: 561–580.
- 1093 Goudarzi M, Berg K, Pieper LM, Schier AF. 2019. Individual long non-coding RNAs have no overt
1094 functions in zebrafish embryogenesis, viability and fertility. *eLife* **8**.
- 1095 Graur D, Zheng Y, Price N, Azevedo RBR, Zufall RA, Elhaik E. 2013. On the immortality of television sets:
1096 “function” in the human genome according to the evolution-free gospel of ENCODE. *Genome*
1097 *Biol Evol* **5**: 578–590.
- 1098 Green CD, Ma Q, Manske GL, Shami AN, Zheng X, Marini S, Moritz L, Sultan C, Gurczynski SJ, Moore BB,
1099 et al. 2018. A comprehensive roadmap of murine spermatogenesis defined by single-cell RNA-
1100 Seq. *Dev Cell* **46**: 651-667.e10.
- 1101 Groff AF, Sanchez-Gomez DB, Soruco MML, Gerhardinger C, Barutcu AR, Li E, Elcavage L, Plana O,
1102 Sanchez LV, Lee JC, et al. 2016. In vivo characterization of Linc-p21 reveals functional cis-
1103 regulatory DNA elements. *Cell Rep* **16**: 2178–2186.
- 1104 Grote P, Herrmann BG. 2015. Long noncoding RNAs in organogenesis: making the difference. *Trends*
1105 *Genet TIG* **31**: 329–335.

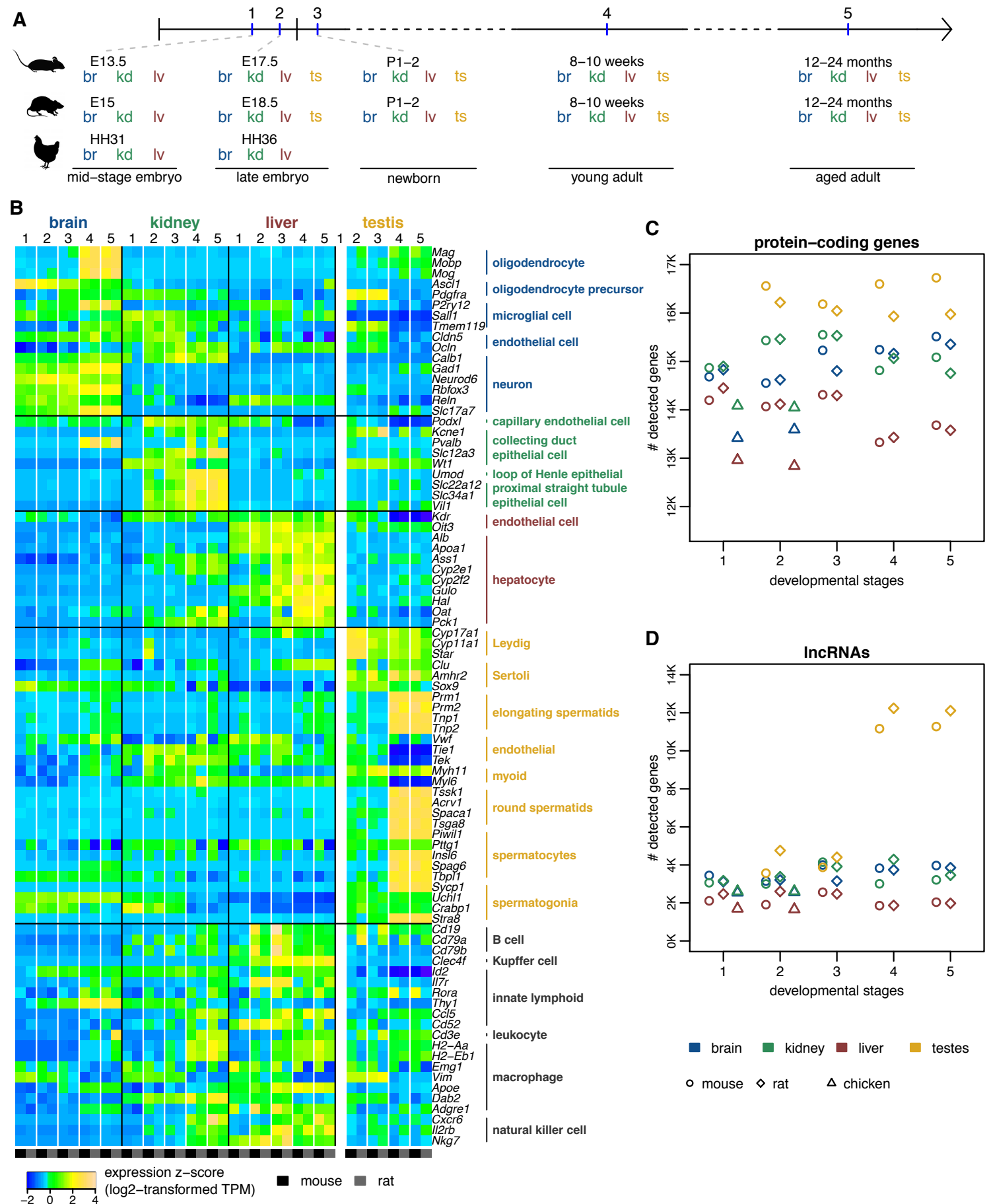
- 1106 Grote P, Wittler L, Hendrix D, Koch F, Währisch S, Beisaw A, Macura K, Bläss G, Kellis M, Werber M, et
1107 al. 2013. The tissue-specific lncRNA Fendrr is an essential regulator of heart and body wall
1108 development in the mouse. *Dev Cell* **24**: 206–214.
- 1109 Guttman M, Amit I, Garber M, French C, Lin MF, Feldser D, Huarte M, Zuk O, Carey BW, Cassady JP, et
1110 al. 2009. Chromatin signature reveals over a thousand highly conserved large non-coding RNAs
1111 in mammals. *Nature* **458**: 223–227.
- 1112 Haerty W, Ponting CP. 2014. No gene in the genome makes sense except in the light of evolution. *Annu
1113 Rev Genomics Hum Genet* **15**: 71–92.
- 1114 Haerty W, Ponting CP. 2015. Unexpected selection to retain high GC content and splicing enhancers
1115 within exons of multiexonic lncRNA loci. *RNA N Y N* **21**: 333–346.
- 1116 Hamburger V, Hamilton HL. 1951. A series of normal stages in the development of the chick embryo. *J
1117 Morphol* **88**: 49–92.
- 1118 Herrero J, Muffato M, Beal K, Fitzgerald S, Gordon L, Pignatelli M, Vilella AJ, Searle SMJ, Amode R, Brent
1119 S, et al. 2016. Ensembl comparative genomics resources. *Database J Biol Databases Curation*
1120 **2016**.
- 1121 Hezroni H, Koppstein D, Schwartz MG, Avrutin A, Bartel DP, Ulitsky I. 2015. Principles of long noncoding
1122 RNA evolution derived from direct comparison of transcriptomes in 17 species. *Cell Rep* **11**:
1123 1110–1122.
- 1124 Iyer MK, Niknafs YS, Malik R, Singhal U, Sahu A, Hosono Y, Barrette TR, Prensner JR, Evans JR, Zhao S,
1125 et al. 2015. The landscape of long noncoding RNAs in the human transcriptome. *Nat Genet* **47**:
1126 199–208.
- 1127 Kaessmann H. 2010. Origins, evolution, and phenotypic impact of new genes. *Genome Res* **20**: 1313–
1128 1326.
- 1129 Kathleen Baxter K, Uittenbogaard M, Yoon J, Chiaramello A. 2009. The neurogenic basic helix-loop-
1130 helix transcription factor NeuroD6 concomitantly increases mitochondrial mass and regulates
1131 cytoskeletal organization in the early stages of neuronal differentiation. *ASN Neuro* **1**.
- 1132 Khalil AM, Guttman M, Huarte M, Garber M, Raj A, Rivea Morales D, Thomas K, Presser A, Bernstein
1133 BE, van Oudenaarden A, et al. 2009. Many human large intergenic noncoding RNAs associate
1134 with chromatin-modifying complexes and affect gene expression. *Proc Natl Acad Sci U S A* **106**:
1135 11667–11672.
- 1136 Kim D, Langmead B, Salzberg SL. 2015. HISAT: a fast spliced aligner with low memory requirements.
1137 *Nat Methods* **12**: 357–60.
- 1138 Kutter C, Watt S, Stefflova K, Wilson MD, Goncalves A, Ponting CP, Odom DT, Marques AC. 2012. Rapid
1139 turnover of long noncoding RNAs and the evolution of gene expression. *PLoS Genet* **8**:
1140 e1002841.
- 1141 Latos PA, Pauler FM, Koerner MV, Şenergin HB, Hudson QJ, Stocsits RR, Allhoff W, Stricker SH, Klement
1142 RM, Warczok KE, et al. 2012. Airn transcriptional overlap, but not its lncRNA products, induces
1143 imprinted Igf2r silencing. *Science* **338**: 1469–1472.

- 1144 Liao B-Y, Scott NM, Zhang J. 2006. Impacts of gene essentiality, expression pattern, and gene
1145 compactness on the evolutionary rate of mammalian proteins. *Mol Biol Evol* **23**: 2072–2080.
- 1146 Liao Y, Smyth GK, Shi W. 2019. The R package Rsubread is easier, faster, cheaper and better for
1147 alignment and quantification of RNA sequencing reads. *Nucleic Acids Res.*
- 1148 Lin MF, Carlson JW, Crosby MA, Matthews BB, Yu C, Park S, Wan KH, Schroeder AJ, Gramates LS, St
1149 Pierre SE, et al. 2007. Revisiting the protein-coding gene catalog of *Drosophila melanogaster*
1150 using 12 fly genomes. *Genome Res* **17**: 1823–1836.
- 1151 Lin MF, Jungreis I, Kellis M. 2011. PhyloCSF: a comparative genomics method to distinguish protein
1152 coding and non-coding regions. *Bioinforma Oxf Engl* **27**: i275-282.
- 1153 Liu SJ, Nowakowski TJ, Pollen AA, Lui JH, Horlbeck MA, Attenello FJ, He D, Weissman JS, Kriegstein AR,
1154 Diaz AA, et al. 2016. Single-cell analysis of long non-coding RNAs in the developing human
1155 neocortex. *Genome Biol* **17**: 67.
- 1156 Love MI, Huber W, Anders S. 2014. Moderated estimation of fold change and dispersion for RNA-seq
1157 data with DESeq2. *Genome Biol* **15**: 550.
- 1158 Marques AC, Hughes J, Graham B, Kowalczyk MS, Higgs DR, Ponting CP. 2013. Chromatin signatures at
1159 transcriptional start sites separate two equally populated yet distinct classes of intergenic long
1160 noncoding RNAs. *Genome Biol* **14**: R131.
- 1161 McMahon AP. 2016. Development of the Mammalian Kidney. *Curr Top Dev Biol* **117**: 31–64.
- 1162 Nakagaki BN, Mafra K, de Carvalho É, Lopes ME, Carvalho-Gontijo R, de Castro-Oliveira HM, Campolina-
1163 Silva GH, de Miranda CDM, Antunes MM, Silva ACC, et al. 2018. Immune and metabolic shifts
1164 during neonatal development reprogram liver identity and function. *J Hepatol* **69**: 1294–1307.
- 1165 Necsulea A, Soumillon M, Warnefors M, Liechti A, Daish T, Grutzner F, Kaessmann H. 2014. The
1166 evolution of lncRNA repertoires and expression patterns in tetrapods. *Nature* **505**: 635–640.
- 1167 Ørom UA, Derrien T, Beringer M, Gumireddy K, Gardini A, Bussotti G, Lai F, Zytnicki M, Notredame C,
1168 Huang Q, et al. 2010. Long noncoding RNAs with enhancer-like function in human cells. *Cell*
1169 **143**: 46–58.
- 1170 Perteau M, Perteau GM, Antonescu CM, Chang T-C, Mendell JT, Salzberg SL. 2015. StringTie enables
1171 improved reconstruction of a transcriptome from RNA-seq reads. *Nat Biotechnol* **33**: 290–5.
- 1172 Perteau M, Shumate A, Perteau G, Varabyou A, Breitwieser FP, Chang Y-C, Madugundu AK, Pandey A,
1173 Salzberg SL. 2018. CHESS: a new human gene catalog curated from thousands of large-scale
1174 RNA sequencing experiments reveals extensive transcriptional noise. *Genome Biol* **19**: 208.
- 1175 Ponjavic J, Ponting CP, Lunter G. 2007. Functionality or transcriptional noise? Evidence for selection
1176 within long noncoding RNAs. *Genome Res* **17**: 556–65.
- 1177 R Core Team. 2018. *R: A Language and Environment for Statistical Computing*. [https://www.R-
1178 project.org/](https://www.R-project.org/).
- 1179 Ramsköld D, Wang ET, Burge CB, Sandberg R. 2009. An abundance of ubiquitously expressed genes
1180 revealed by tissue transcriptome sequence data. *PLoS Comput Biol* **5**: e1000598.

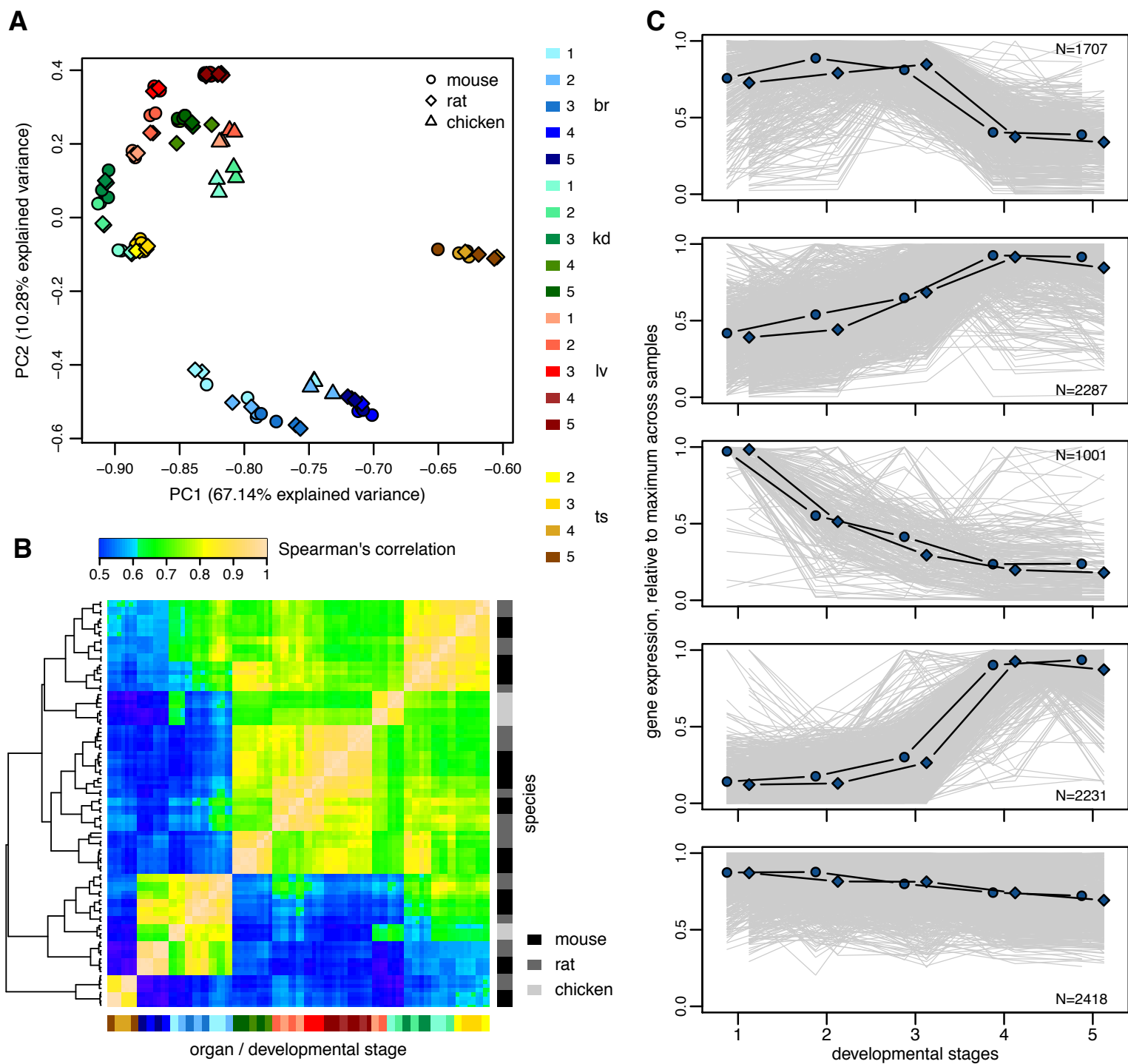
- 1181 Rinn JL, Kertesz M, Wang JK, Squazzo SL, Xu X, Bruggmann SA, Goodnough LH, Helms JA, Farnham PJ,
1182 Segal E, et al. 2007. Functional demarcation of active and silent chromatin domains in human
1183 HOX loci by noncoding RNAs. *Cell* **129**: 1311–1323.
- 1184 Sauvageau M, Goff LA, Lodato S, Bonev B, Groff AF, Gerhardinger C, Sanchez-Gomez DB, Hacisuleyman
1185 E, Li E, Spence M, et al. 2013. Multiple knockout mouse models reveal lincRNAs are required
1186 for life and brain development. *eLife* **2**: e01749.
- 1187 Schüler A, Ghanbarian AT, Hurst LD. 2014. Purifying selection on splice-related motifs, not expression
1188 level nor RNA folding, explains nearly all constraint on human lincRNAs. *Mol Biol Evol* **31**: 3164–
1189 3183.
- 1190 Siepel A, Bejerano G, Pedersen JS, Hinrichs AS, Hou M, Rosenbloom K, Clawson H, Spieth J, Hillier LW,
1191 Richards S, et al. 2005. Evolutionarily conserved elements in vertebrate, insect, worm, and
1192 yeast genomes. *Genome Res* **15**: 1034–50.
- 1193 Smedley D, Haider S, Ballester B, Holland R, London D, Thorisson G, Kasprzyk A. 2009. BioMart--
1194 biological queries made easy. *BMC Genomics* **10**: 22.
- 1195 Smit AF., Hubley R, Green P. 2003. *RepeatMasker Open-4.0*. <http://www.repeatmasker.org>.
- 1196 Soumillon M, Necsulea A, Weier M, Brawand D, Zhang X, Gu H, Barthès P, Kokkinaki M, Nef S, Gnirke
1197 A, et al. 2013. Cellular source and mechanisms of high transcriptome complexity in the
1198 mammalian testis. *Cell Rep* **3**: 2179–2190.
- 1199 Tabula Muris Consortium. 2018. Single-cell transcriptomics of 20 mouse organs creates a Tabula Muris.
1200 *Nature* **562**: 367–372.
- 1201 Theiler K. 1989. *The house mouse: atlas of embryonic development*. Springer-Verlag, Berlin Heidelberg
1202 <https://www.springer.com/la/book/9783642884207>.
- 1203 The UniProt Consortium. 2017. UniProt: the universal protein knowledgebase. *Nucleic Acids Res* **45**:
1204 D158–D169.
- 1205 Uebbing S, Konzer A, Xu L, Backström N, Brunström B, Bergquist J, Ellegren H. 2015. Quantitative mass
1206 spectrometry reveals partial translational regulation for dosage compensation in chicken. *Mol*
1207 *Biol Evol* **32**: 2716–2725.
- 1208 Ulitsky I. 2016. Evolution to the rescue: using comparative genomics to understand long non-coding
1209 RNAs. *Nat Rev Genet* **17**: 601–614.
- 1210 Ulitsky I, Shkumatava A, Jan CH, Sive H, Bartel DP. 2011. Conserved function of lincRNAs in vertebrate
1211 embryonic development despite rapid sequence evolution. *Cell* **147**: 1537–1550.
- 1212 Villar D, Berthelot C, Aldridge S, Rayner TF, Lukk M, Pignatelli M, Park TJ, Deaville R, Erichsen JT,
1213 Jasinska AJ, et al. 2015. Enhancer evolution across 20 mammalian species. *Cell* **160**: 554–566.
- 1214 Washietl S, Kellis M, Garber M. 2014. Evolutionary dynamics and tissue specificity of human long
1215 noncoding RNAs in six mammals. *Genome Res* **24**: 616–28.
- 1216 Zakany J, Darbellay F, Mascrez B, Necsulea A, Duboule D. 2017. Control of growth and gut maturation
1217 by HoxD genes and the associated lincRNA Haglr. *Proc Natl Acad Sci U S A* **114**: E9290–E9299.

1218

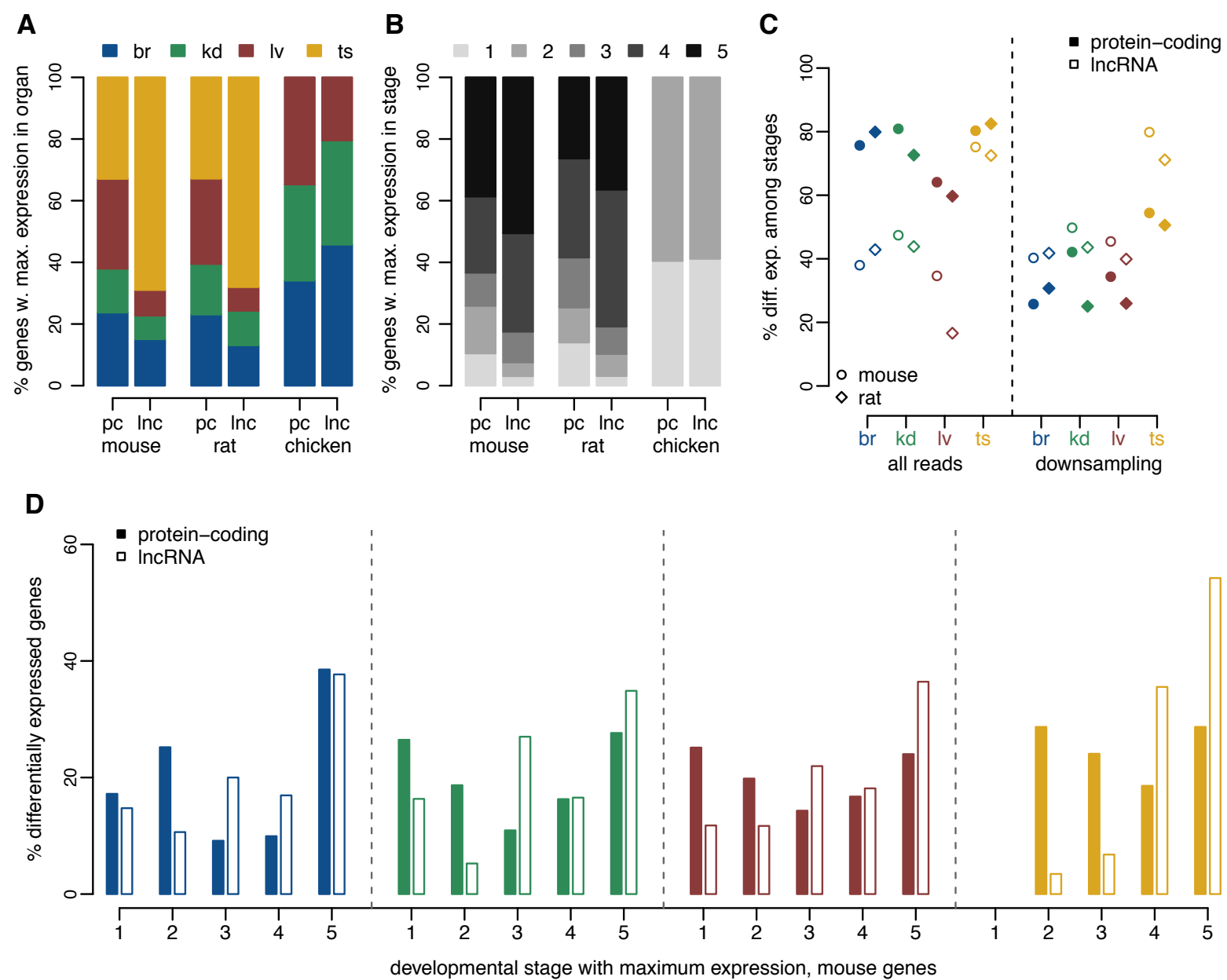
Darbellay and Necsulea, Figure 1



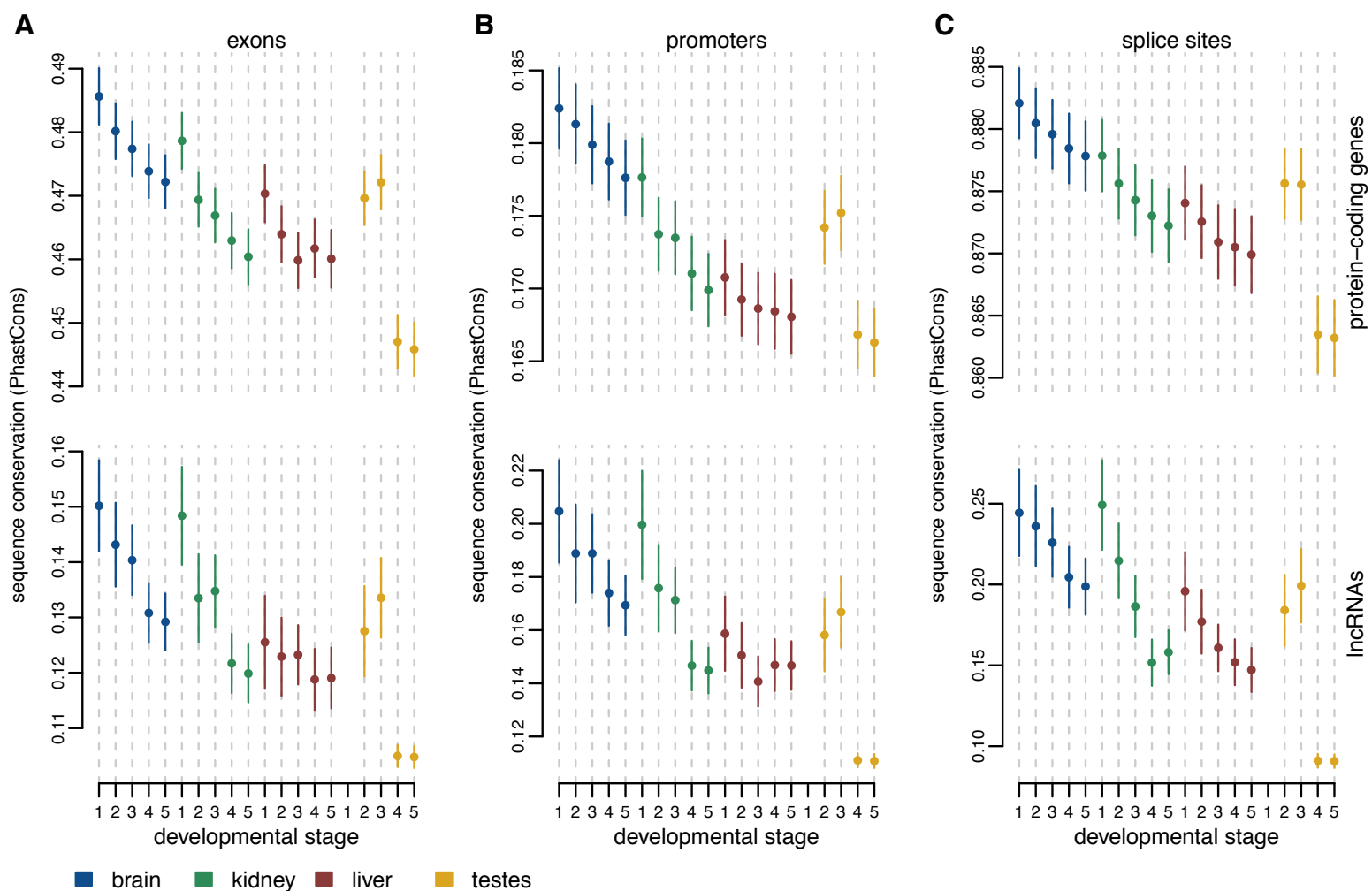
Darbellay and Necsulea, Figure 2



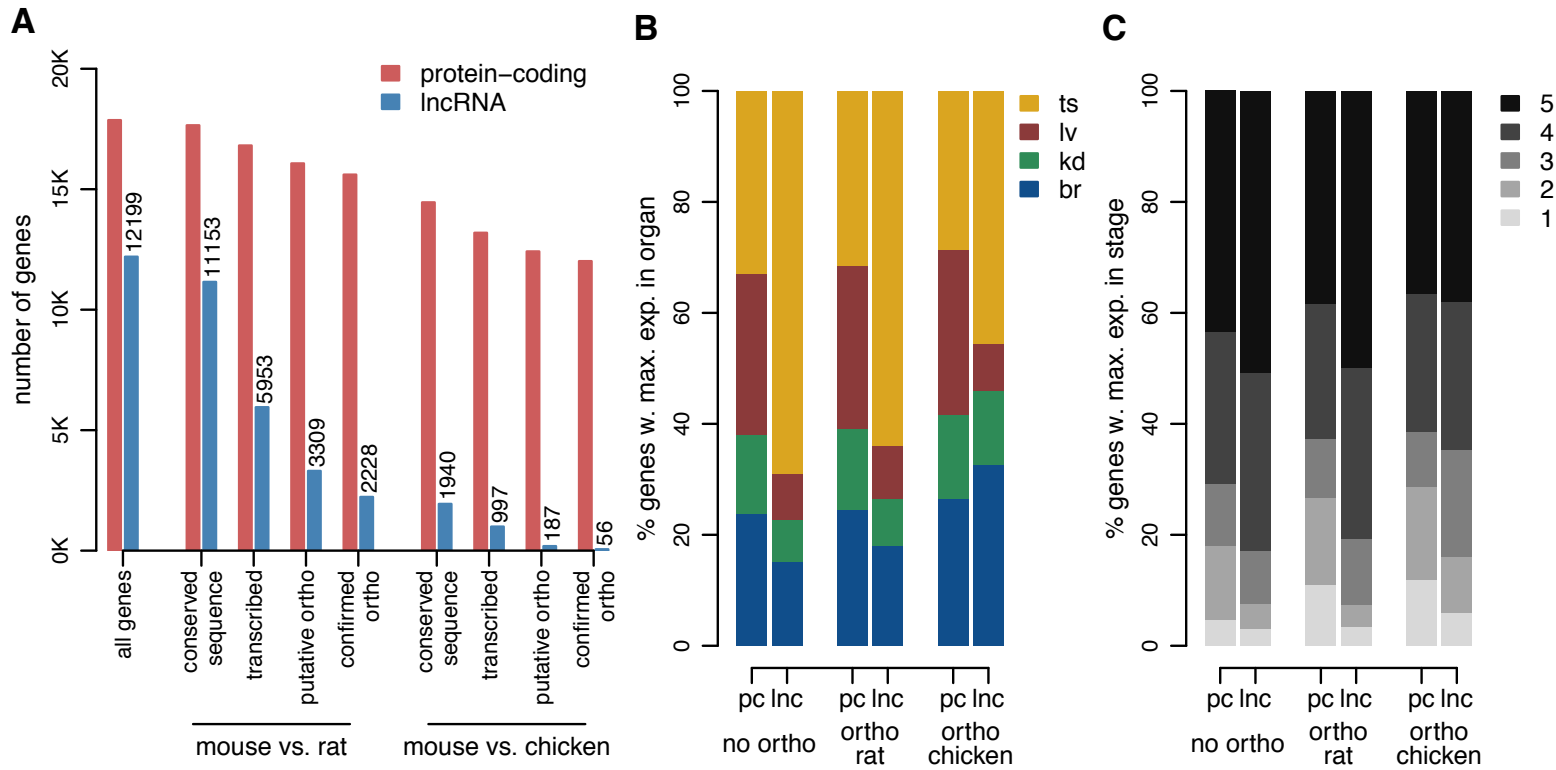
Darbellay and Necsulea, Figure 3



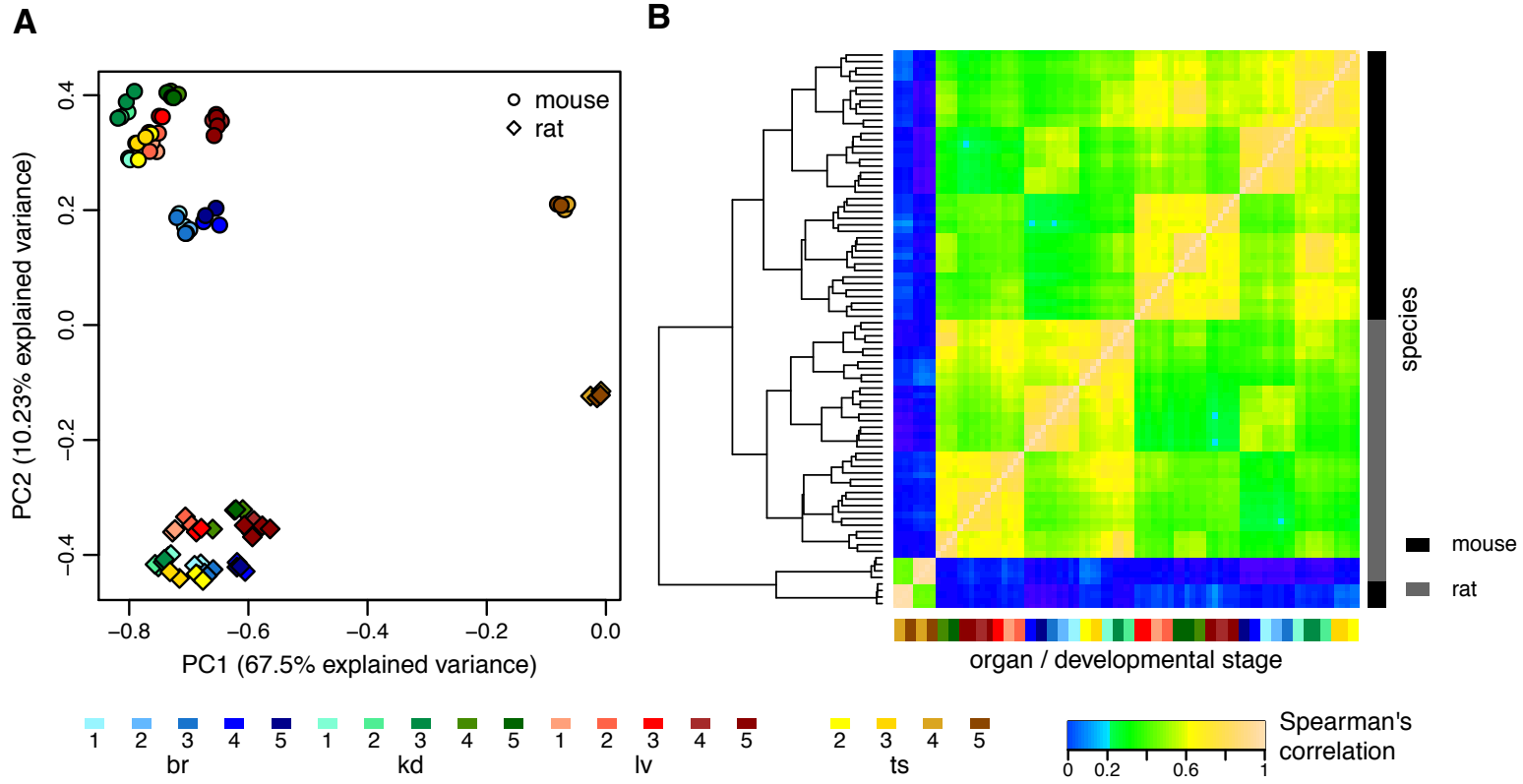
Darbellay and Necsulea, Figure 4



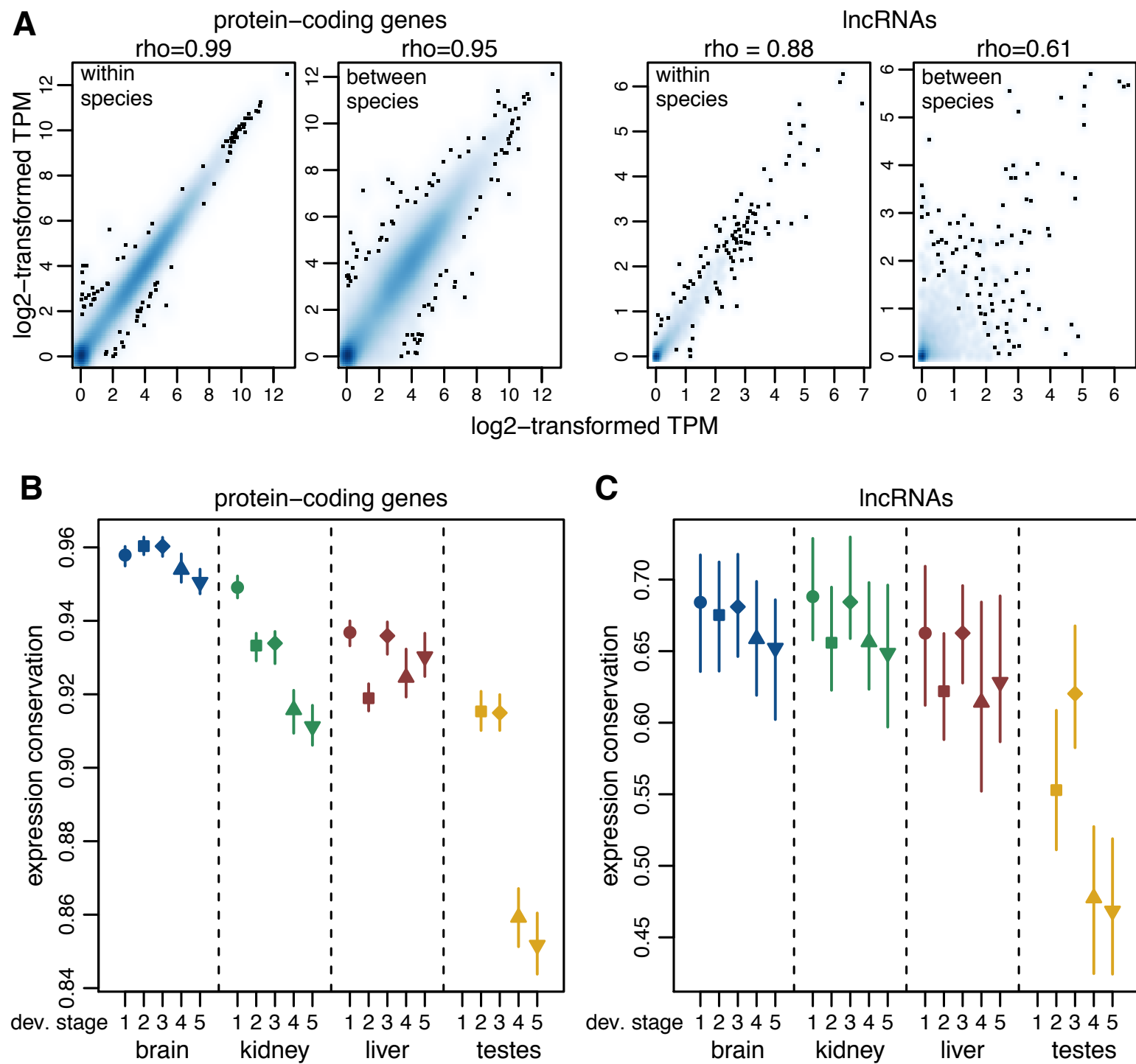
Darbellay and Necsulea, Figure 5



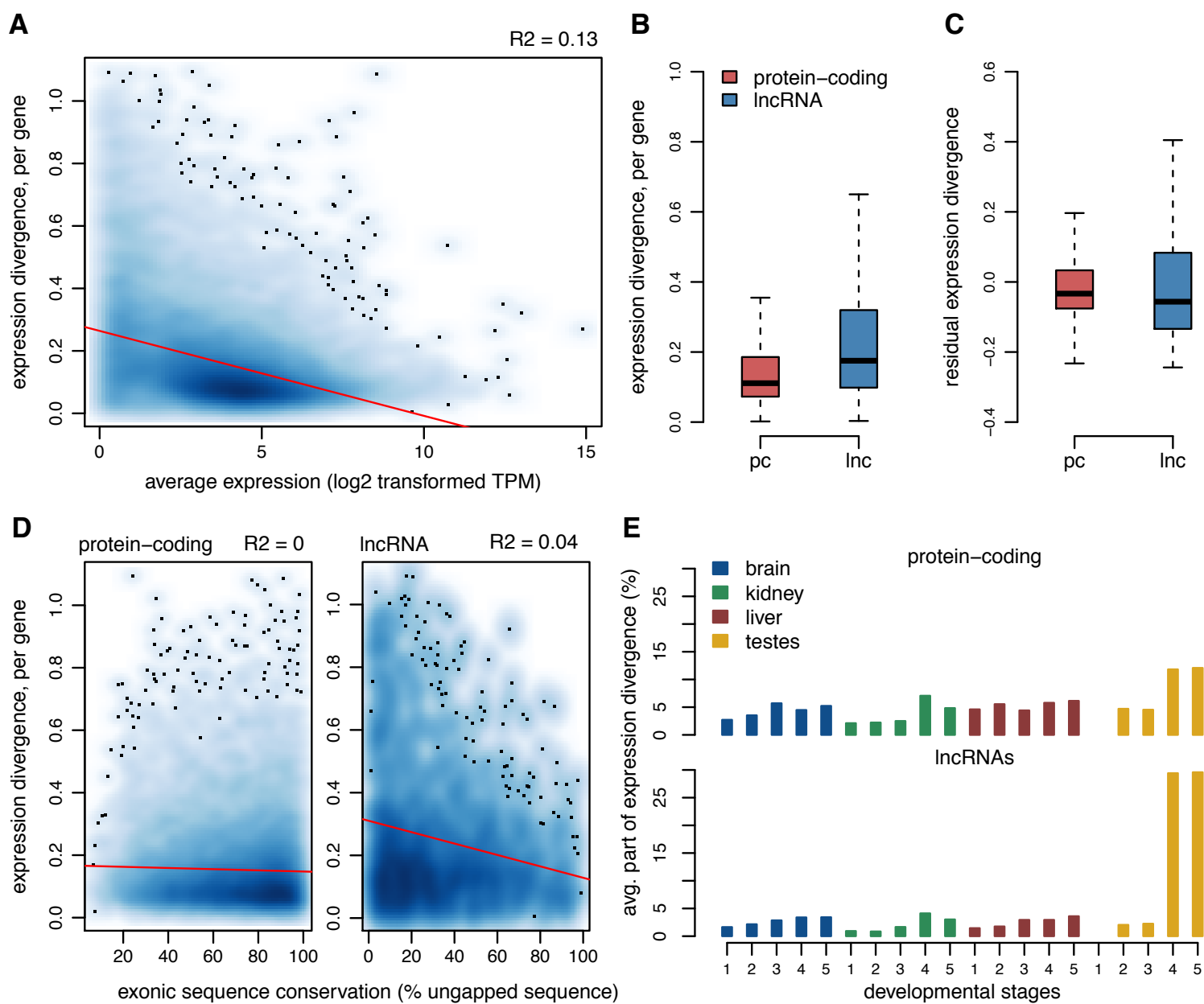
Darbellay and Necsulea, Figure 6



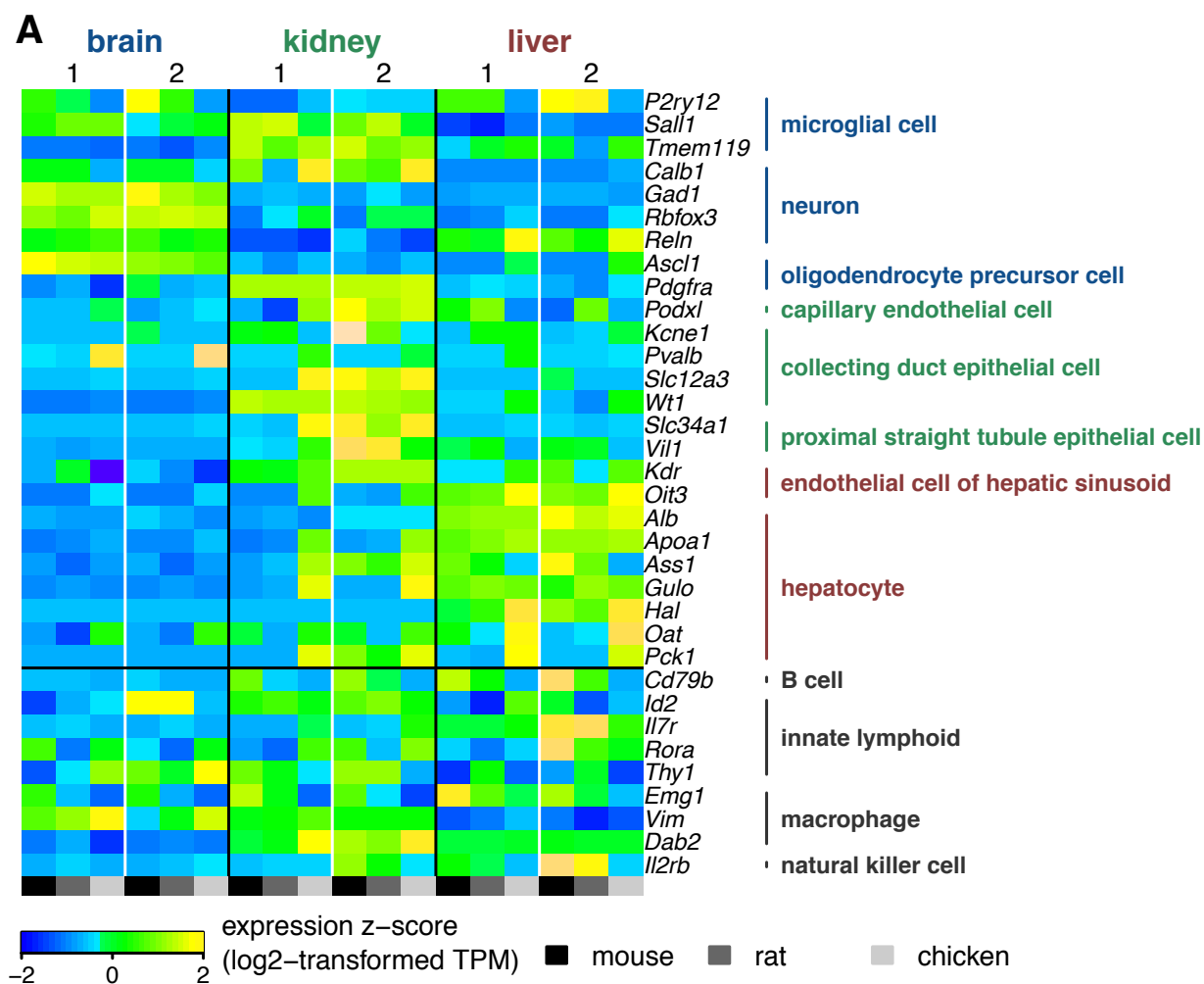
Darbellay and Necsulea, Figure 7



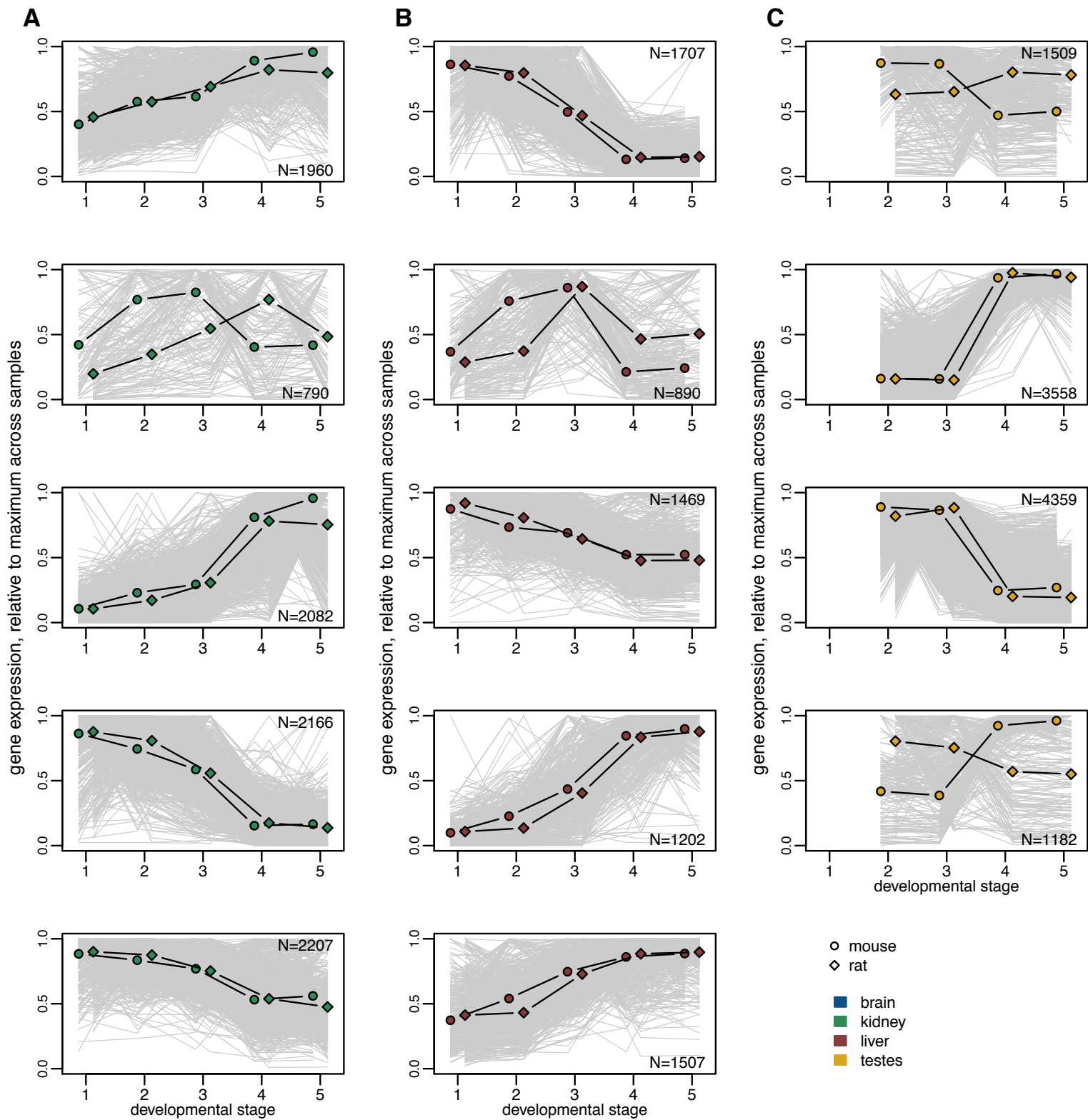
Darbellay and Necsulea, Figure 8



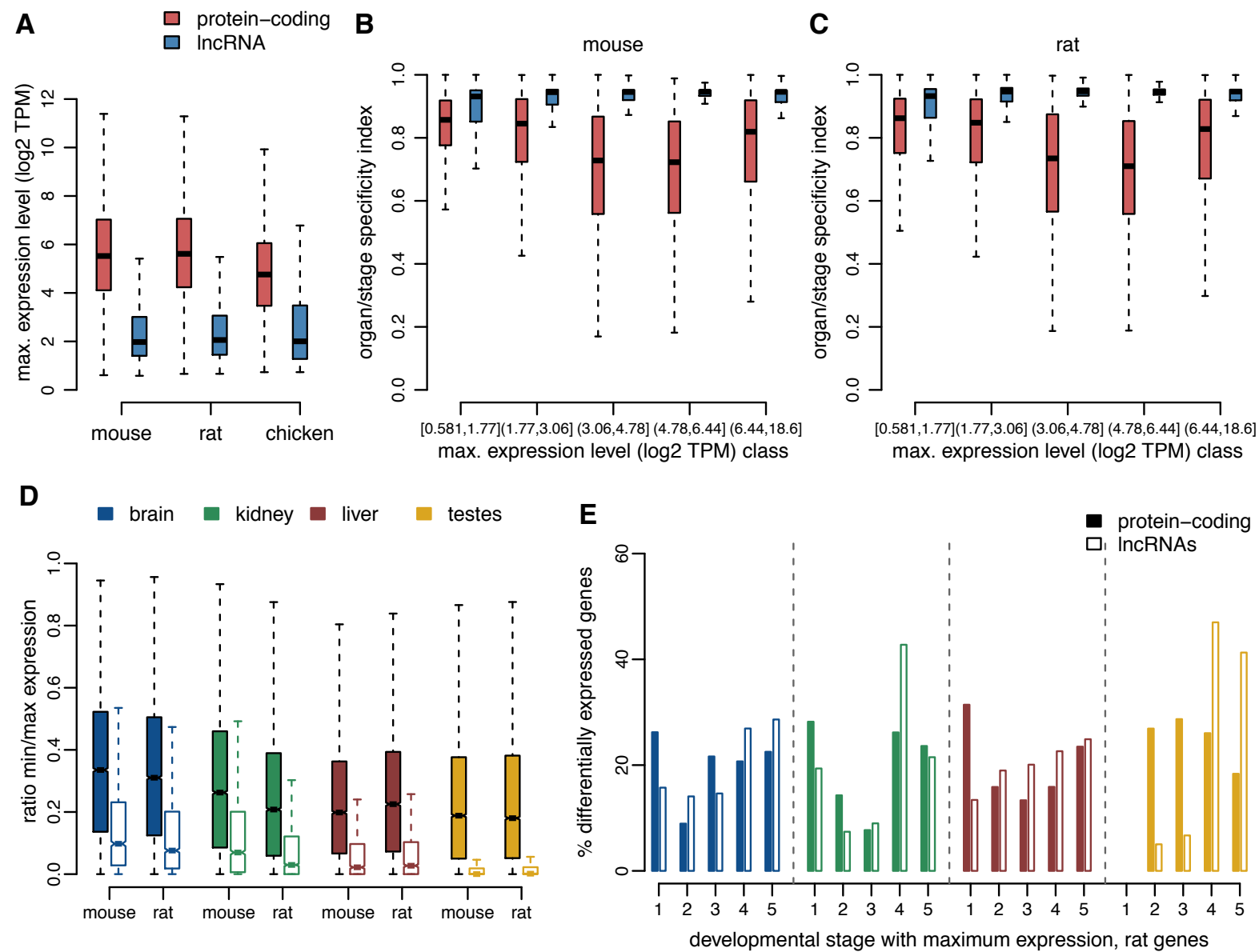
Darbellay and Necsulea, Supplementary Figure 1



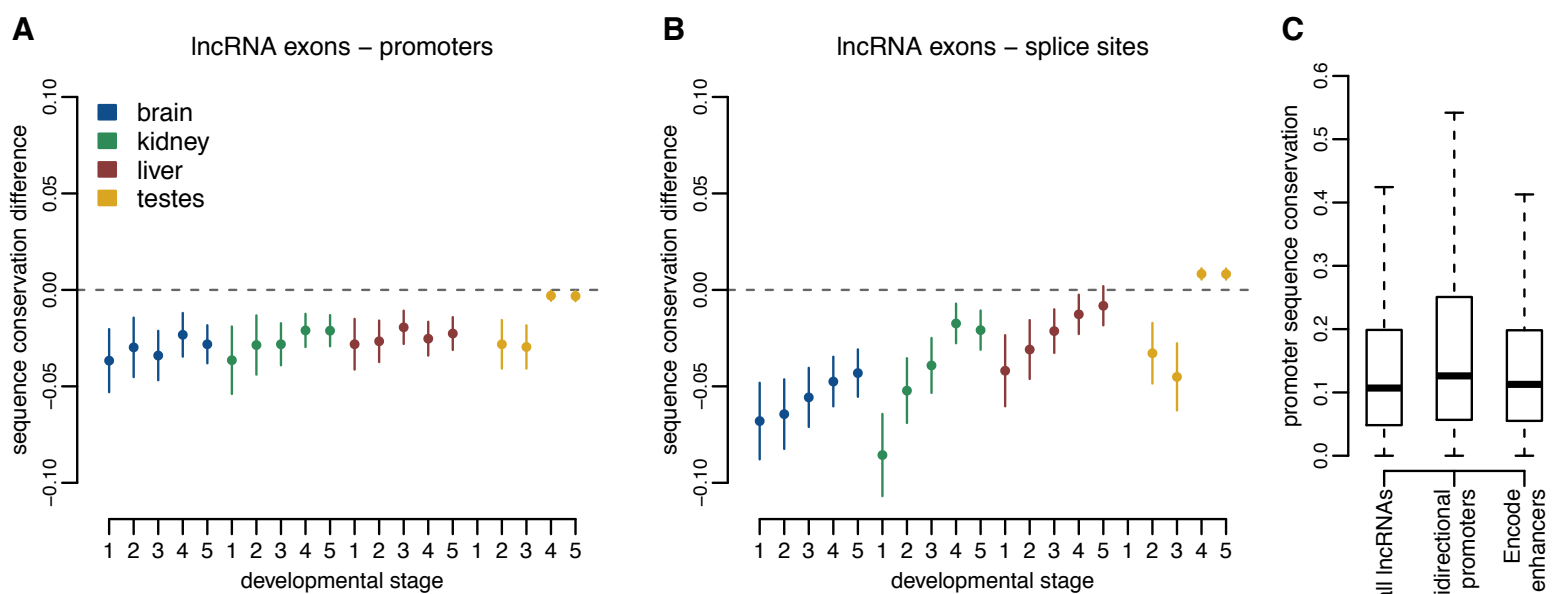
Darbellay and Necsulea, Supplementary Figure 2



Darbellay and Necsulea, Supplementary Figure 3

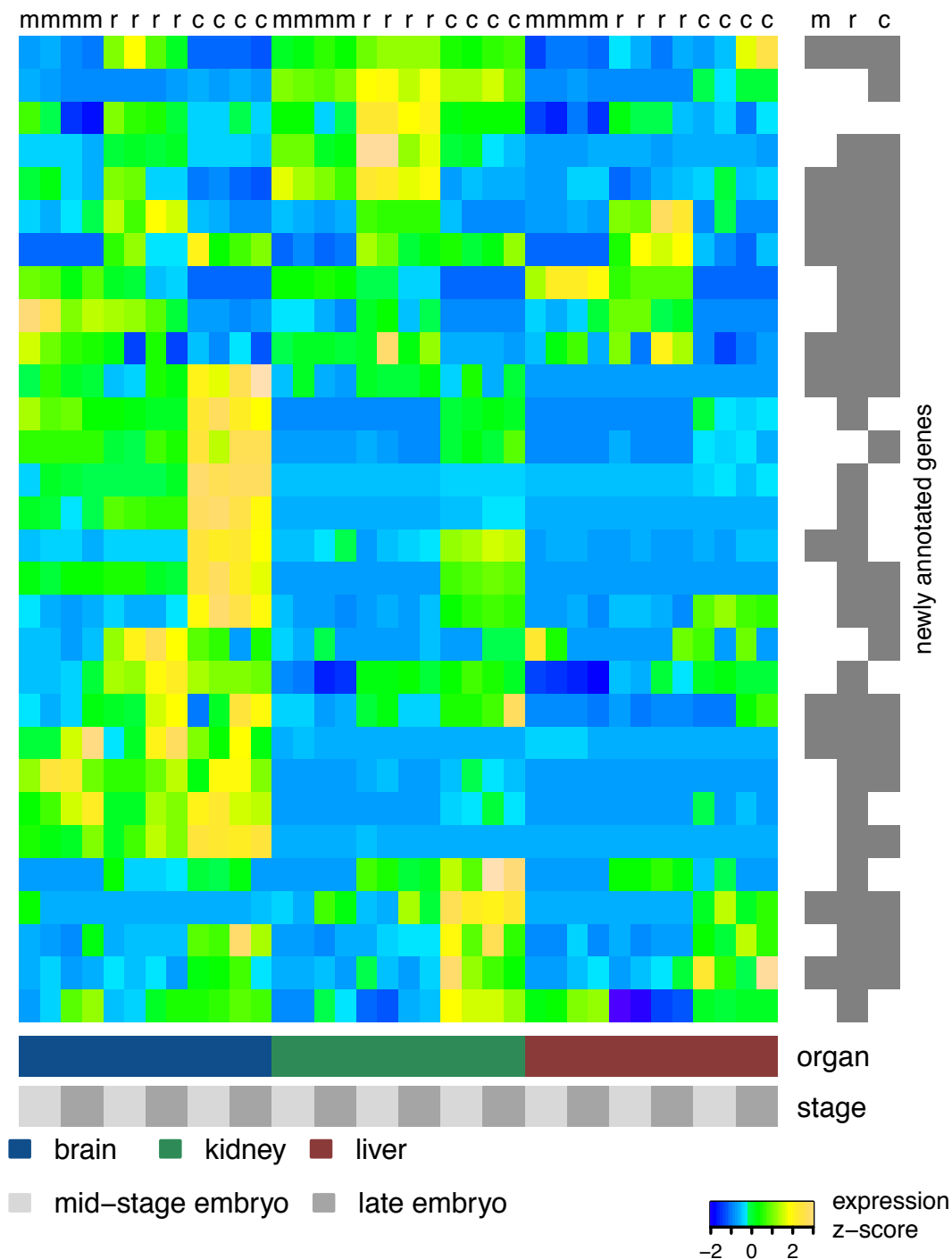


Darbellay and Necsulea, Supplementary Figure 4

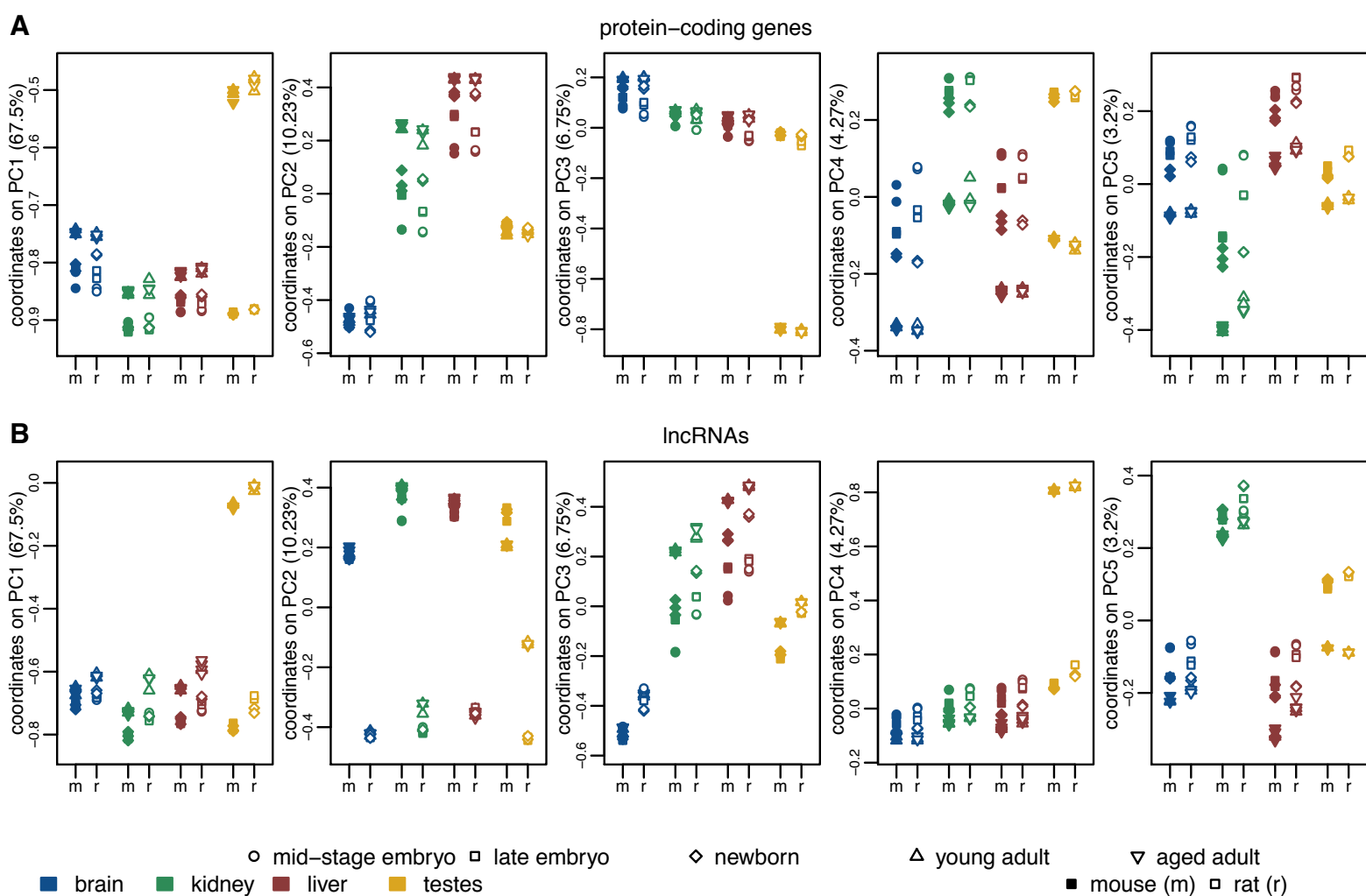


Darbellay and Necsulea, Supplementary Figure 5

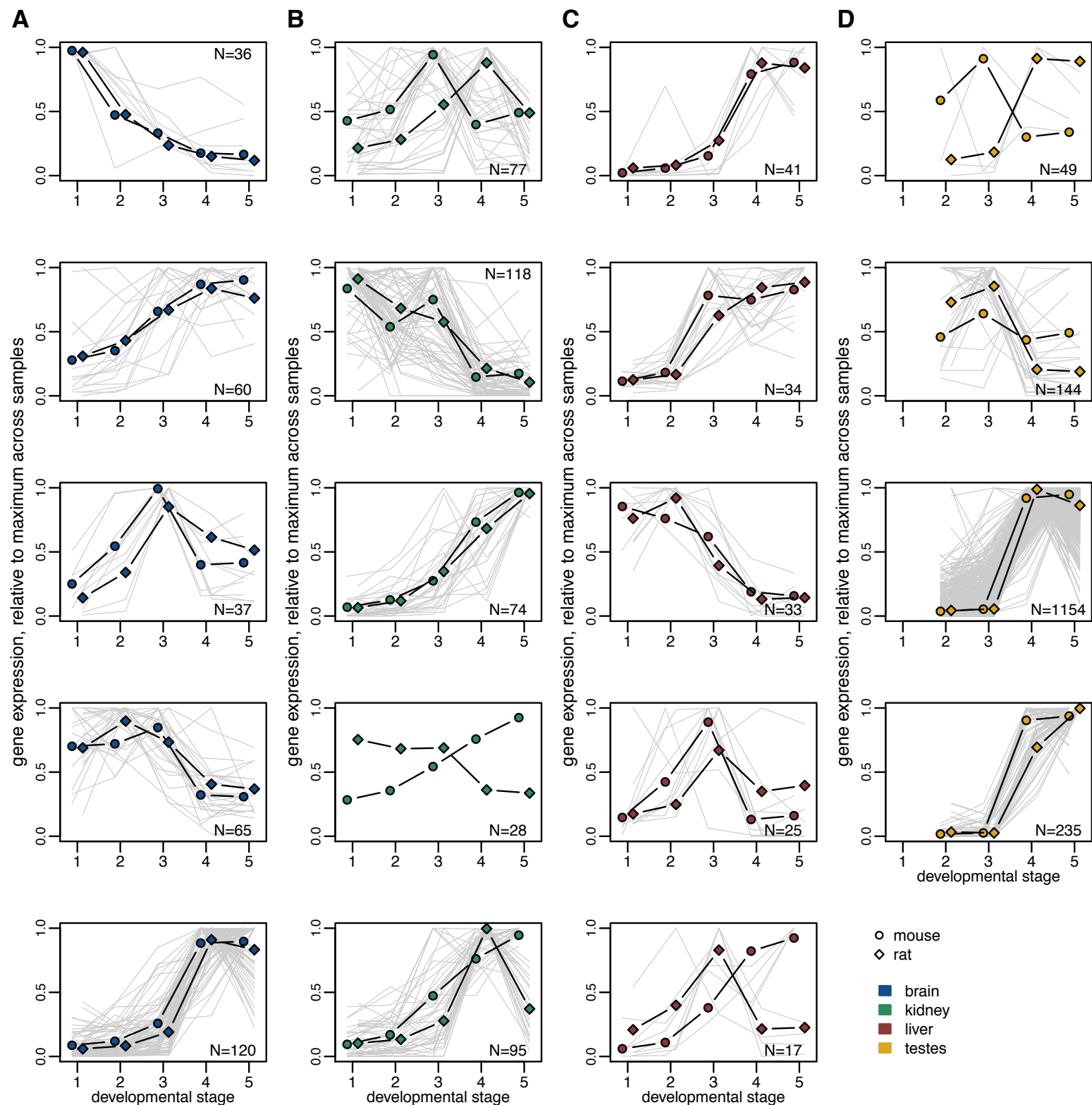
A



Darbellay and Necsulea, Supplementary Figure 6

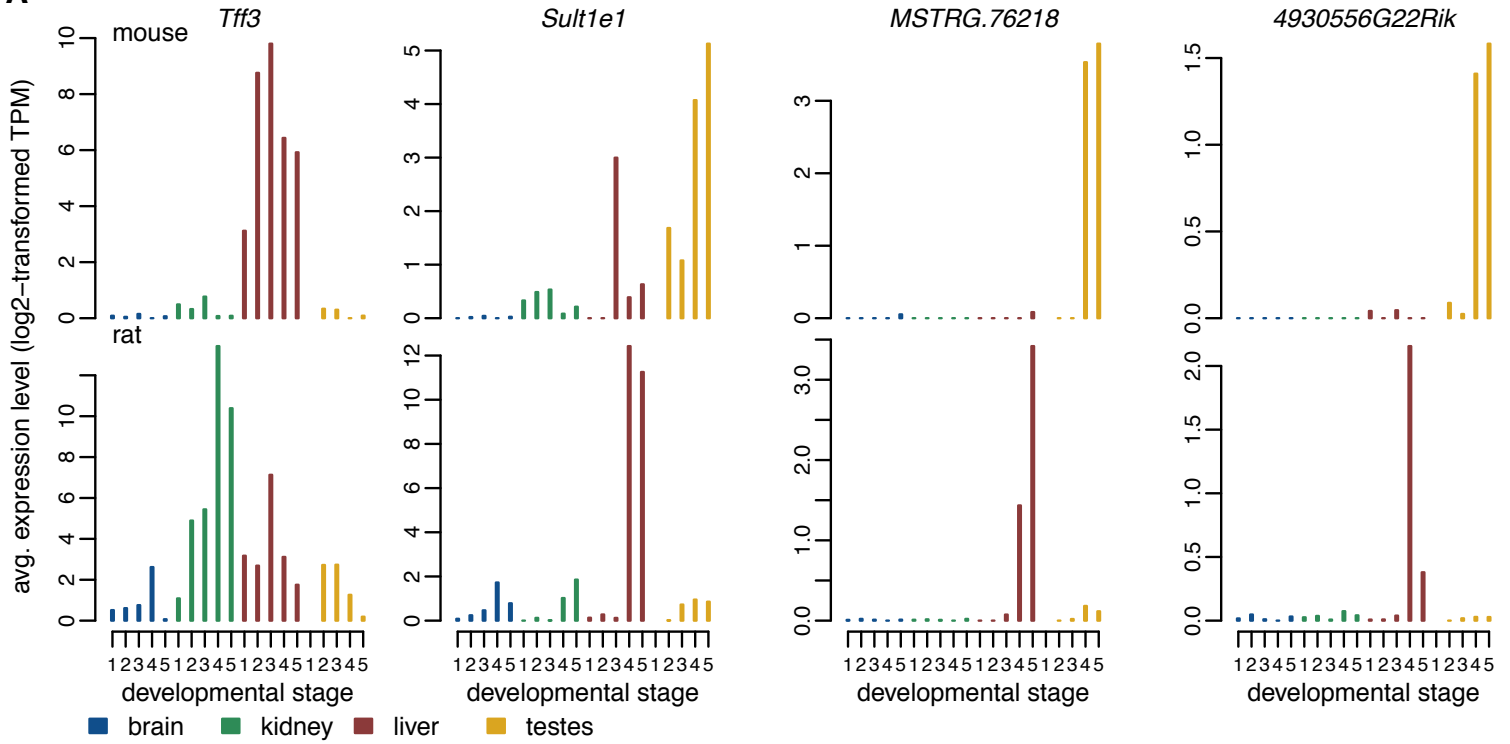


Darbellay and Necsulea, Supplementary Figure 7

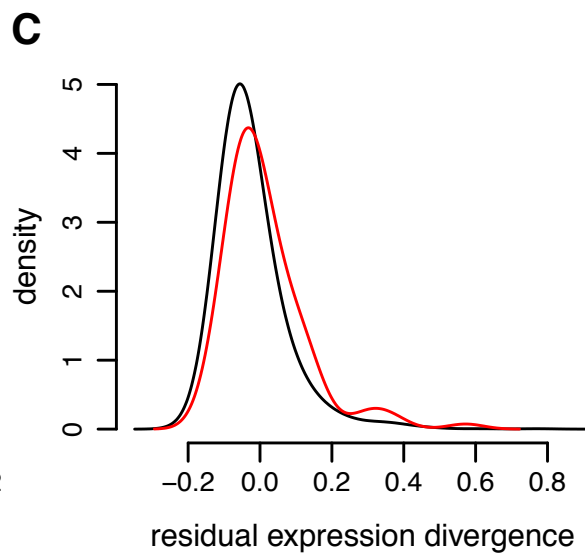
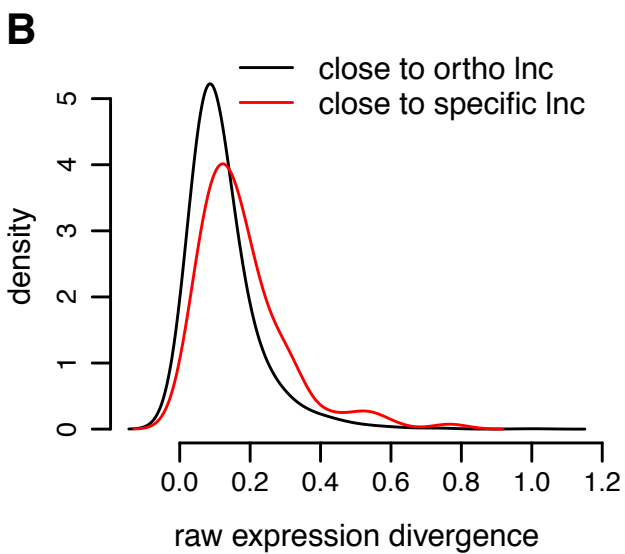
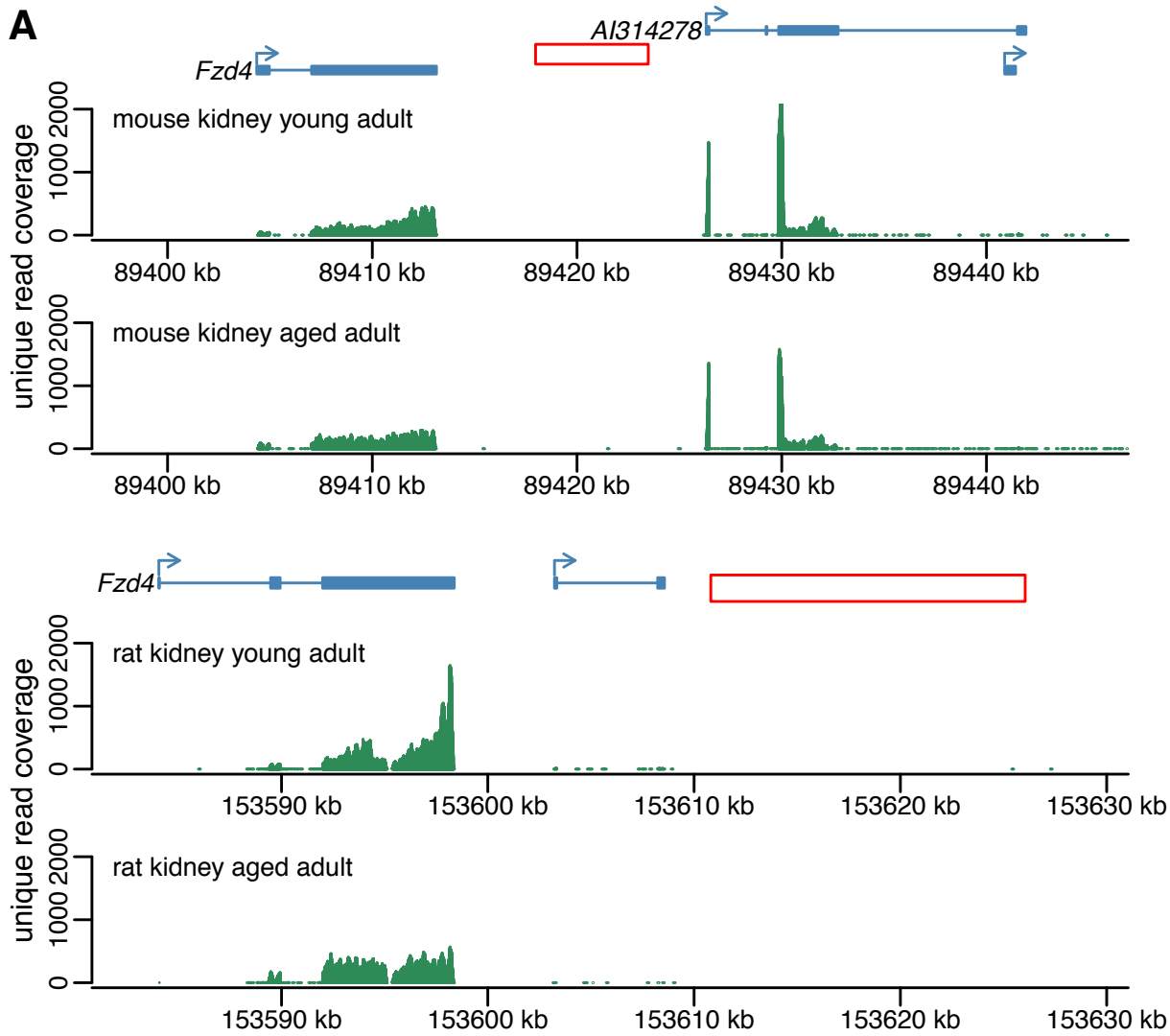


Darbelay and Necsulea, Supplementary Figure 8

A



Darbella and Necsulea, Supplementary Figure 9



Darbella and Necsulea, Supplementary Figure 10

